Tensors for Data Processing

Theory, Methods, and Applications

Edited by

Yipeng Liu

School of Information and Communication Engineering
University of Electronic Science and Technology
of China (UESTC)
Chengdu, China

ACADEMIC PRESS
An imprint of Elsevier

Academic Press is an imprint of Elsevier
125 London Wall, London EC2Y 5AS, United Kingdom
525 B Street, Suite 1650, San Diego, CA 92101, United States
50 Hampshire Street, 5th Floor, Cambridge, MA 02139, United States
The Boulevard, Langford Lane, Kidlington, Oxford OX5 1GB, United Kingdom

Notices

Knowledge and best practice in this field are constantly changing. As new research and experience broaden our understanding, changes in research methods, professional practices, or medical treatment may become necessary.

Practitioners and researchers must always rely on their own experience and knowledge in evaluating and using any information, methods, compounds, or experiments described herein. In using such information or methods they should be mindful of their own safety and the safety of others, including parties for whom they have a professional responsibility.

To the fullest extent of the law, neither the Publisher nor the authors, contributors, or editors, assume any liability for any injury and/or damage to persons or property as a matter of products liability, negligence or otherwise, or from any use or operation of any methods, products, instructions, or ideas contained in the material herein.

Library of Congress Cataloging-in-Publication Data
A catalog record for this book is available from the Library of Congress

British Library Cataloguing-in-Publication Data
A catalogue record for this book is available from the British Library

ISBN: 978-0-12-824447-0

For information on all Academic Press publications
visit our website at https://www.elsevier.com/books-and-journals

Publisher: Mara Conner
Acquisitions Editor: Tim Pitts
Editorial Project Manager: Charlotte Rowley
Production Project Manager: Prem Kumar Kaliamoorthi
Designer: Miles Hitchen

Typeset by VTeX

CHAPTER

Tensors for neuroimaging

12

A review on applications of tensors to unravel the mysteries of the brain

Aybüke Erol and Borbála Hunyadi
Circuits and Systems, Department of Microelectronics, Delft University of Technology, Delft, The Netherlands

CONTENTS

12.1 Introduction

Understanding how the brain works has always been a challenge for humankind, for both cognitive and clinical purposes. Neurosurgery is believed to be the oldest medical specialty, dating back to ancient times [1]. Today, neuroscience combines the advances in neuroimaging technology and signal processing, and while the mystery

Tensors for Data Processing. https://doi.org/10.1016/B978-0-12-824447-0.00018-2

of the brain keeps being unraveled, we have achieved many breakthroughs in diagnostic tools and treatments of neurological or psychosomatic diseases.

In fact, the relationship between neuroscience and engineering technologies is two-sided. Certainly, engineering is involved in every aspect of neuroimaging, and in the development of diagnostic tools and medical care systems. However, understanding of the brain's anatomy and functioning has also inspired the making of such engineering tools, and even more. The most straightforward, yet powerful example of this phenomenon is given by artificial neural networks, which mimic the human nervous system for artificial intelligence tasks. Artificial neural networks are used in various fields, including medicine, nanotechnology, telecommunications, autonomous vehicles, art, and finance [2].

Overall, modeling of the structure and function of the brain gains more and more attention every day. In this review, we look into where tensors stand on the way to understanding the mechanisms behind brain function. The main motivation for the use of tensors to model brain signals follows from the fact that brain signals are inherently large-scale and can hold various modes such as time, space, frequency, channel, experimental condition, modality, trial, and subject. The interactions across different modes can only be fully captured by expanding the order of simple space-time representations, and as such call for tensor-based (multiway) methods instead of matrix-based (two-way) methods. Tensors are increasingly used in a broad range of neuroimaging applications, from filling in missing or noisy recordings to feature extraction and classification for brain–computer interfaces (BCIs).

The rest of this chapter is organized as follows. First, fundamentals of the most common neuroimaging modalities are provided. Each neuroimaging modality grasps the brain data based on different biophysical principles (such as electrical or magnetic outcomes of neuronal transmission) and presents them in different fashions for different objectives (such as temporal evolution of brain images in order to reveal the functioning of neural circuits, unlike structural neuroimaging, which focuses on the brain anatomy). These fundamentals are necessary to understand the nature of the input data for accurate modeling and further processing.

Next, the convenience of using tensor-based modeling of neural signals and images is discussed. This section focuses on the multiway nature and the complex organization of the brain and explains how tensors essentially fit brain data representations.

This is followed by a section highlighting the most common tensor decomposition structures, which will be referred to in the upcoming sections. These structures include canonical polyadic (CP) decomposition, Tucker decomposition, and block term decomposition (BTD), together with their commonly used variants.

Subsequently, various applications of tensors in the neuroimaging literature are presented. This section is organized in parallel with an intuitive ordering of the main steps in data analysis pipelines, ranging from preprocessing strategies (such as denoising and dimensionality reduction) to classification of brain data for the purpose of BCIs. In the end, a summary of the considered tensor-based methods is provided, along with the most common practical challenges that are encountered while using

these methods. Several strategies that can be used to tackle the presented challenges are also mentioned.

Last but not least, we point out future challenges that await medical technology and the widespread adoption of tensor tools to address these challenges.

12.2 Neuroimaging modalities

A diagram of main neuroimaging modalities is provided in Fig. 12.1. This review will investigate these modalities from the perspective of how tensors can be useful to capture the multiway nature of acquired brain signals for various applications.

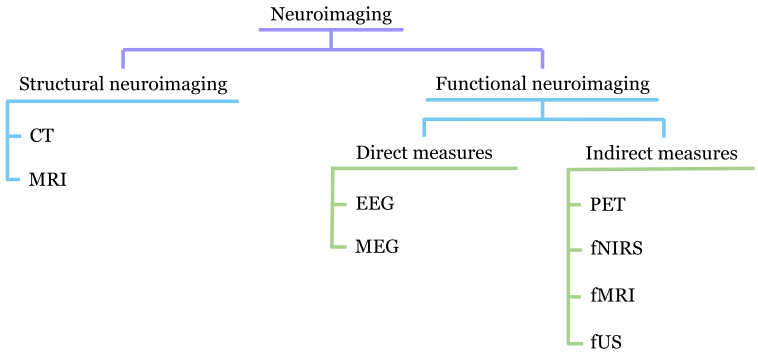

FIGURE 12.1

Categorization of neuroimaging modalities.

The area of neuroimaging can be divided into two main fields, namely structural and functional neuroimaging [3]. Structural imaging deals with the analysis of anatomical properties of the brain and is useful for diagnosing intracranial lesions such as tumors. The earliest technique used for imaging the brain structure is computed tomography (CT), which utilizes X-rays to visualize brain slices [4]. Later, magnetic resonance imaging (MRI), which uses powerful magnets instead of ionizing radiation, has replaced CT, offering greater contrast between normal and abnormal brain tissue [5]. There exist several variants of MRI such as magnetic resonance spectroscopic imaging (MRSI), which includes an extra dimension for spectroscopic information besides the MRI data. Other variants include T1- (and T2-)weighted MRI, perfusion-weighted imaging (PWI), diffusion-weighted imaging (DWI), and diffusion tensor imaging (DTI), which further enhance the contrast in MR images by incorporating the effect of tissue relaxation times, the hemodynamic status of tissues, tissue water diffusion rates, and tissue water anisotropies, respectively [6,7].

On the other hand, functional imaging is used to identify brain areas and processes that are associated with performing a particular cognitive or behavioral task. Information flow in the brain while processing a task is controlled by the firing of neurons

via both electrical and chemical signals [8]. Provided in Fig. 12.2 is an illustration showing the effects of neuronal activity together with the modalities that make use of those effects for neuroimaging.

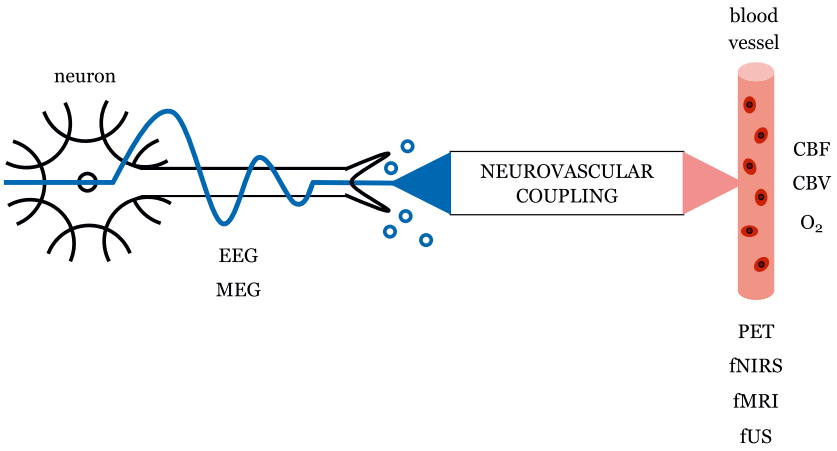

FIGURE 12.2

Functional neuroimaging modalities, which are discussed in this review in detail, are shown in relation to neurovascular coupling. Neurovascular coupling describes the relationship between neuronal activity (which takes place using both electrical and chemical signals) and the resulting changes in blood flow. EEG and MEG directly measure neuronal activity whereas PET, fNIRS, fMRI, and fUS provide an indirect measure through neurovascular coupling.

The neuronal activity of the brain can be recorded directly by electroencephalography (EEG) and magnetoencephalography (MEG) in the form of aggregated postsynaptic potentials of larger neuronal populations. EEG is the oldest functional brain imaging technique, with the first reported human EEG dating back to 1929. In EEG, the electrical activity of neurons is detected via electrodes placed along or below (intracranial EEG or electrocorticography [ECoG]) the scalp [9]. On the other hand, MEG records the magnetic field produced by this electrical activity using magnetometers, which are most commonly selected as superconducting quantum unit interference devices [10].

The indirect measures of neuronal activity rely on a phenomenon known as neurovascular coupling. When a brain region becomes active, it starts to consume more glucose and oxygen. These changes are met by an increasing blood flow to the region, known as the hemodynamic response. Neurovascular coupling describes this interaction between local neuronal activity and cerebral blood flow (CBF) [11] and forms the basis of many functional neuroimaging techniques including positron emission tomography (PET), functional near-infrared spectroscopy (fNIRS), functional magnetic resonance imaging (fMRI), and functional ultrasound (fUS) (Fig. 12.2).

PET measures the alterations in glucose levels in response to metabolic activity by injection of radioactive tracers to the brain which are attached to glucose

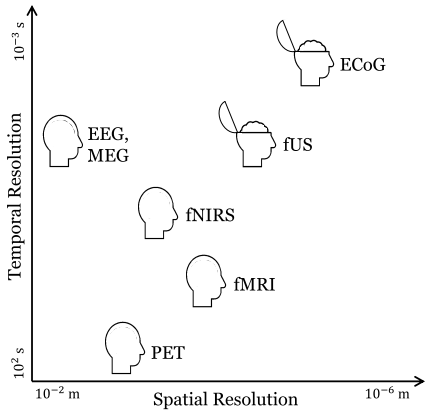

FIGURE 12.3

Functional neuroimaging modalities with their temporal and spatial resolutions, where an opened skull refers to invasive imaging [16].

and absorbed by the bloodstream [12]. Meanwhile, the changes in oxygenation of hemoglobin in red blood cells can be detected by fNIRS and fMRI. In fNIRS, near-infrared light is used to track hemodynamic changes based on the differential optical properties of hemoglobin states [13]. The magnetic properties of hemoglobin are affected as well by the amount of oxygen that the cells carry, resulting in the blood oxygen level-dependent (BOLD) signal detected by fMRI via electromagnets. Since the early 1990s, fMRI has come to dominate brain mapping research due to its non-invasive nature (requiring no injections or surgery) and high spatial resolution [14]. Nevertheless, fUS, a recently developed neuroimaging technique, is able to image the brain with higher spatiotemporal resolution than fMRI, yet at lower cost. In fUS imaging, ultrasound waves are transmitted to the brain through a cranial window and the strength of the reflected waves is directly proportional to the number of moving red blood cells in the local region, i.e., the local CBF or cerebral blood volume (CBV) [15]. The temporal and spatial resolutions of the aforementioned functional neuroimaging modalities are compared in Fig. 12.3.

12.3 Multidimensionality of the brain

Brain activity exists and spreads in time and space. Hence, temporal and/or spatial modes follow straightforwardly while describing brain data [17]. In structural neuroimaging, the objective is to only visualize brain anatomy; therefore, the collected brain data have only spatial information. These visualizations can be brought in pixels of 2D slices or voxels of 3D volumes. On the other hand, in functional neuroimaging, the functioning of the brain is to be monitored, which means that temporal informa-

tion is involved as well as spatial information. In the case of EEG and MEG, spatial information is depicted by channel locations instead of pixels or voxels.

Many studies have also considered the frequency mode and worked on space-time-frequency models of neural signals [89]. Furthermore, the increasing use of multiple subjects, experimental conditions, modalities, or trials have naturally introduced other modes in brain data representations. Such multiway models are naturally fit to multidimensional arrays, named as tensors. Fig. 12.4 shows several examples of third-order tensor models (although higher orders are also possible, only third-order tensors are given for visualization) used in the neuroimaging literature.

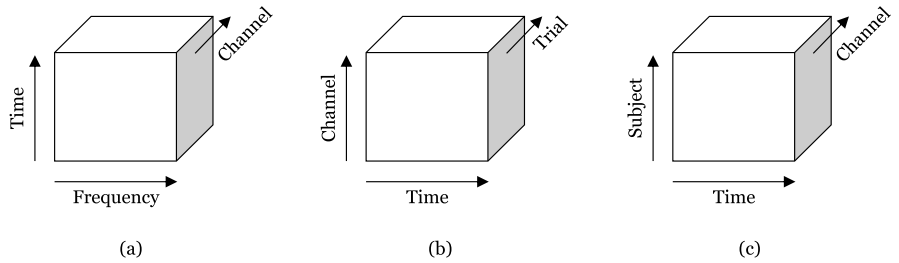

FIGURE 12.4

Examples of third-order tensor representations used in neuroimaging literature. The models provided in (a), (b), and (c) are utilized in [89], [43], and [18], respectively.

It is possible and quite common to unfold such modes of a tensor to obtain a matrix, so that well-established decomposition methods that are set in the 2D framework such as principal component analysis (PCA) or independent component analysis (ICA) can be utilized. PCA is a technique to identify modes of variation in a data matrix by defining orthogonal subspaces of the data. The most common tool to perform PCA is singular value decomposition (SVD). SVD uniquely decomposes an input matrix to its orthogonal singular (i.e., basis) vectors, which are ordered from most to least significant in terms of how much variance in the data matrix they account for. Hence, PCA can be obtained by truncation of the less important singular vectors from the original SVD subspaces. On the other hand, the goal of ICA is to find a set of statistically independent basis vectors whose linear combination (i.e., the mixing matrix) returns the data matrix.

However, both methods require any extra mode, such as subjects, to be represented in the input data matrix by concatenation in time or space. Such matricization of a tensor causes underestimation of existing interactions between the folded modes [19] and neglects variations over the unfolded mode, i.e., time courses or spatial maps that are common across the new modes (e.g., subjects) are obtained. Group ICA methods can partially address this problem by later predicting the individual maps or courses using back-projection, but the multidimensional structure of data is not reflected in the estimation stage itself [20]. In addition, the assumptions made by PCA and ICA, i.e., orthogonality and independence, respectively, may be physically irrelevant [90].

On the contrary, there is a trend to tensorize data that were originally in matrix form. For instance, fusing cumulant information with the covariance of the measurement matrix and stacking several time-lagged covariance matrices have been shown to improve ICA results [21]. Such tensorization, or imposing a priori information on neural data [103], leads to decompositions that exhibit certain structures, such as in the form of Hankel [103] or Toeplitz [81] blocks. These structures often change across modes and/or factors, which is much easier to incorporate using tensor models.

Last but not least, many conventional approaches require an a priori selection of a region of interest along one or more modes, such as a time window [22], an anatomical area [23], or a frequency band [24], to be examined. On the other hand, tensors can handle the whole dimensionality of the brain and can be applied in a completely data-driven manner.

To summarize, tensors are the natural representations of neural signals, considering both the way they are acquired and the complexity of brain activity itself. As such, tensors also facilitate drawing neurophysiologically meaningful conclusions [25]. Accompanied by the escalating development of mathematical tools to perform tensor-based analyses, the ability of tensors to fairly model and process the large-scale and multidimensional neural data favors the utilization of tensors in neuroimaging applications.

12.4 Tensor decomposition structures

As one of the most important tools in 2D analysis, SVD (along with PCA) has been at the core of data analysis since more than a century ago. Using SVD, any matrix $\mathbf{X}$ can be factorized as follows [26]:

$$\mathbf{X} = \mathbf{U}\boldsymbol{\Sigma}\mathbf{V}^{\mathrm{H}}, \tag{12.1}$$

where $\mathbf{U}$ and $\mathbf{V}$ are unitary matrices whose columns stand for the left and right singular vectors of $\mathbf{X}$, respectively, and $\boldsymbol{\Sigma}$ is a diagonal matrix. The diagonal elements of $\boldsymbol{\Sigma}$, denoted by $\sigma_i \geq 0$, appear in decreasing order and are called the singular values of $\mathbf{X}$. If $\mathbf{X}$ is real, $\mathbf{U}$ and $\mathbf{V}$ are real orthogonal matrices. Eq. (12.1) can also be expressed using the outer product as follows:

$$\mathbf{X} = \sum_i \sigma_i \mathbf{u}_i \circ \mathbf{v}_i, \tag{12.2}$$

where $\mathbf{u}_i$ and $\mathbf{v}_i$ show the i-th column of $\mathbf{U}$ and $\mathbf{V}$, respectively.

SVD is used in all areas of science, engineering, and statistics [27]. However, as mentioned in the previous section, reducing the dimensionality of a multiway array by unfolding causes a loss of information and variance over the unfolded mode(s). Therefore, tensor decomposition methods are necessary for analyzing multiway data.

The goal of tensor decomposition is to approximate an original input tensor using a smaller number of parameters by expressing it in terms of lower-dimensional

subspaces. This section provides a short introduction to the main tensor decomposition structures that are different generalizations of matrix SVD to tensors and which will also be referred to in the later parts of this chapter. These structures are CP decomposition (CPD), also known as CANDECOMP/PARAFAC analysis, Tucker decomposition, BTD, and their commonly used variants. In order to be able to formulate these decompositions, various product operations defined on tensors are also presented.

12.4.1 Product operations for tensors

There are four product operations defined on tensors which are essential to fully acknowledge the tensor decompositions, as well as many other computations in the tensor framework that are used in various applications, as will be seen in the later sections.

- The outer product of N vectors $\mathbf{u}^{(1)}, \mathbf{u}^{(2)}, ..., \mathbf{u}^{(N)}$ produces a rank-1 tensor $\boldsymbol{\mathcal{X}} \in \mathbb{R}^{I_1 \times I_2 \times ... \times I_N}$ denoted as $\boldsymbol{\mathcal{X}} = \mathbf{u}^{(1)} \circ \mathbf{u}^{(2)} \circ ... \circ \mathbf{u}^{(N)}$. The elements of $\boldsymbol{\mathcal{X}}$ are given by

$$x_{i_1 i_2 ... i_N} = u^{(1)}_{i_1} u^{(2)}_{i_2} ... u^{(N)}_{i_N}. \tag{12.3}$$

- The n-mode (matrix) product of a tensor $\boldsymbol{\mathcal{X}} \in \mathbb{R}^{I_1 \times I_2 \times ... \times I_N}$ and a matrix $\mathbf{U} \in \mathbb{R}^{J \times I_n}$ is given by a tensor $\boldsymbol{\mathcal{Z}} = \boldsymbol{\mathcal{X}} \times_n \mathbf{U}$, whose elements satisfy the following [28]:

$$z_{i_1 ... \, i_{n-1} \, j \, i_{n+1} ... \, i_N} = \sum_{i_n=1}^{I_n} x_{i_1 i_2 ... i_N} u_{j i_n}. \tag{12.4}$$

- The generalization of the n-mode product to two tensors is called a tensor contraction. While an n-mode product is computed along one common dimension (I_n) of a given matrix and tensor, two tensors may share multiple common dimensions, along which contraction is defined. Formally, if two tensors carry common dimension(s) $J_1, J_2, ..., J_M$ such that $\boldsymbol{\mathcal{X}} \in \mathbb{R}^{I_1 \times I_2 \times ... \times I_N \times J_1 \times J_2 \times ... \times J_M}$ and $\boldsymbol{\mathcal{Y}} \in \mathbb{R}^{J_1 \times J_2 \times ... \times J_M \times K_1 \times K_2 \times ... \times K_P}$, then their tensor contraction over the common dimensions $\boldsymbol{\mathcal{Z}} = \boldsymbol{\mathcal{X}} \bullet_{\{J_1, J_2, ..., J_M\}} \boldsymbol{\mathcal{Y}}$ gives

$$z_{i_1 ... i_N k_1 ... k_p} = \sum_{j_1 ... j_M=1}^{J_1 ... J_M} x_{i_1 ... i_N j_1 ... j_M} y_{j_1 ... j_M k_1 ... k_p}. \tag{12.5}$$

- The tensor–tensor product (or t-product) $\boldsymbol{\mathcal{Z}} = \boldsymbol{\mathcal{X}} \star \boldsymbol{\mathcal{Y}}$, $\boldsymbol{\mathcal{Z}} \in \mathbb{R}^{I \times L \times K}$ of two 3D tensors $\boldsymbol{\mathcal{X}} \in \mathbb{R}^{I \times J \times K}$ and $\boldsymbol{\mathcal{Y}} \in \mathbb{R}^{J \times L \times K}$ is defined using convolution as follows [124]:

$$\mathbf{Z}_k = \sum_{k'=1}^{K} \mathbf{X}_{k'} \bullet_{\{J\}} \mathbf{Y}_{k-k'}, \tag{12.6}$$

where $(.)_k = (.)_{::k}$ denotes the k-th frontal slice of the corresponding tensor.

12.4.2 Canonical polyadic decomposition

CPD expresses an input tensor $\boldsymbol{\mathcal{X}}$ of size $I_1 \times I_2 \times ... \times I_N$ as a sum of R rank-1 terms (Fig. 12.5):

$$\boldsymbol{\mathcal{X}} \approx \sum_{r=1}^{R} \mathbf{u}_r^{(1)} \circ \mathbf{u}_r^{(2)} \circ ... \circ \mathbf{u}_r^{(N)}, \tag{12.7}$$

where R gives the rank of the tensor and each term $\mathbf{u}_r^{(n)}, n = 1, 2 \ldots N$, is a column vector of length I_n and gives rise to the factor matrices $\mathbf{U}^{(n)} = [\mathbf{u}_1^{(n)} \ldots \mathbf{u}_R^{(n)}]$.

CPD can be viewed as an extension of SVD (Eq. (12.2)) to higher orders, with the difference that factor matrices are not necessarily orthogonal [29]. CPD is unique under mild constraints [30].

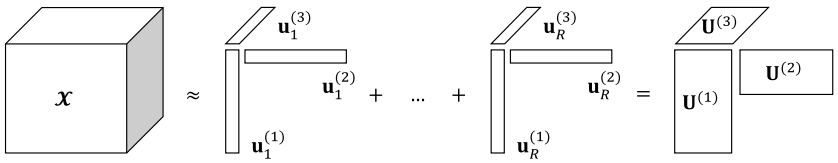

FIGURE 12.5

CPD of a 3D tensor.

For 3D arrays, CPD can also be expressed in matrix notation at each slice $\mathbf{X}_k$ of $\boldsymbol{\mathcal{X}}$ as follows:

$$\mathbf{X}_k \approx \mathbf{U}^{(1)} \mathbf{D}_k (\mathbf{U}^{(2)})^{\mathrm{T}}, \tag{12.8}$$

where $\mathbf{D}_k$ is a diagonal matrix whose diagonal is composed of k-th row elements of $\mathbf{U}^{(3)}$ (Fig. 12.6(a)).

PARAFAC2 is an extension of CPD that is able to represent both regular and irregular tensors which are collections of matrices with changing size along one of the modes (Fig. 12.6(b)). CPD assumes one factor matrix along each mode, meaning that the same set of factor matrices is valid across all slices of a tensor, whereas PARAFAC2 relaxes this constraint by allowing variation across one mode [78]. PARAFAC2 factorizes the input tensor $\boldsymbol{\mathcal{X}}$ at each slice k as $\mathbf{X}_k \approx \mathbf{U}_k^{(1)} \mathbf{D}_k (\mathbf{U}^{(2)})^{\mathrm{T}}$, which is unique under mild constraints [31].

12.4.3 Tucker decomposition

Tucker decomposition (Fig. 12.7) approximates $\boldsymbol{\mathcal{X}}$ as

$$\boldsymbol{\mathcal{X}} \approx \boldsymbol{\mathcal{S}} \times_1 \mathbf{U}^{(1)} \times_2 \mathbf{U}^{(2)} \times_3 \cdots \times_N \mathbf{U}^{(N)}, \tag{12.9}$$

where $\boldsymbol{\mathcal{S}}$ is a core tensor of size $R_1 \times R_2 \times \cdots \times R_N$ ($R_n \leq I_n, \forall n$) and each factor $\mathbf{U}^{(n)}$ is a matrix of size $I_n \times R_n$. Note that Tucker decomposition becomes equivalent to CPD when the core tensor $\boldsymbol{\mathcal{S}}$ is diagonal.

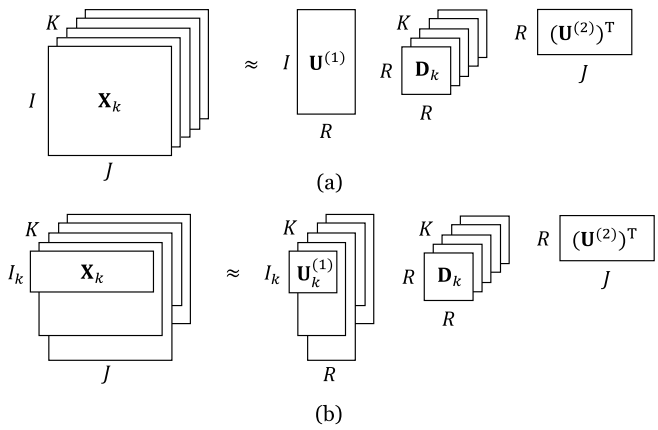

FIGURE 12.6

(a) CPD of a regular 3D tensor and (b) PARAFAC2 decomposition of an irregular 3D tensor, both shown in matrix notation over frontal tensor slices [32].

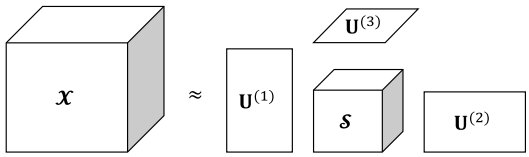

FIGURE 12.7

Tucker decomposition of a 3D tensor.

Referring back to Eq. (12.1), Tucker decomposition with orthogonal factor matrices and an all-orthogonal core tensor corresponds to a multilinear SVD (MLSVD), also known as higher-order SVD (HOSVD) [33]. Owing to the orthogonality conditions, MLSVD is essentially unique [34].

Furthermore, if an input tensor admits to an MLSVD with a diagonal core (i.e., when $\mathcal{S}$ is a diagonal core tensor and factor matrices $\mathbf{U}^{(n)}$ are orthogonal), a decomposition known as tensor SVD is obtained. In the case of 3D tensors, tensor SVD shares the same form as matrix SVD with tensor factors such that

$$\mathcal{X} = \mathcal{U} \star \mathcal{S} \star \mathcal{V}^{\mathrm{T}}, \tag{12.10}$$

where $\mathcal{U}$ and $\mathcal{V}$ are orthogonal tensors and $\mathcal{S}$ is diagonal at each frontal slice (Fig. 12.8) [35].

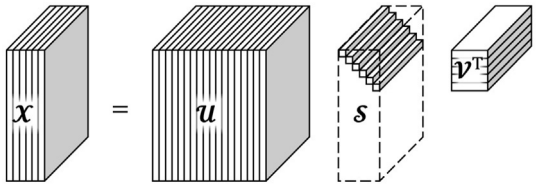

FIGURE 12.8

Tensor SVD of a 3D tensor [36].

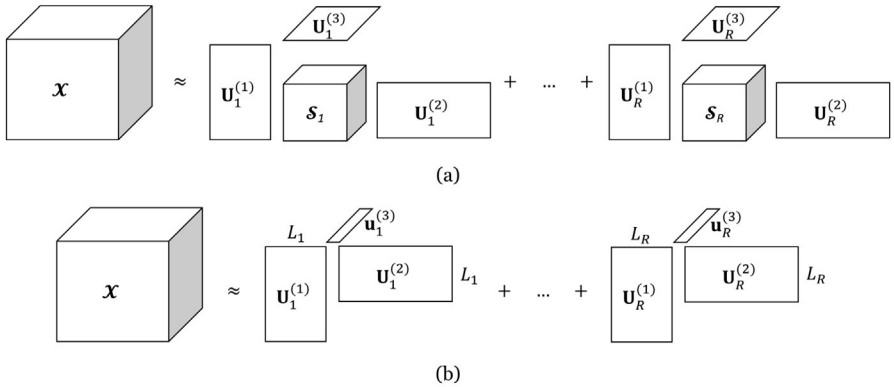

FIGURE 12.9

(a) BTD and (b) rank-$(L_r, L_r, 1)$ BTD of a 3D tensor.

12.4.4 Block term decomposition

BTD can be interpreted as a generalization of CPD where factors can be higher-order tensors (Fig. 12.9(a)) as follows:

$$\mathcal{X} \approx \sum_{r=1}^{R} \mathcal{S}_r \times_1 \mathbf{U}_r^{(1)} \times_2 \mathbf{U}_r^{(2)} \times_3 \cdots \times_N \mathbf{U}_r^{(N)}. \tag{12.11}$$

A special case of BTD, known as rank-$(L_r, L_r, 1)$ BTD, decomposes a 3D input tensor into multilinear rank-$(L_r, L_r, 1)$ terms (Fig. 12.9(b)). The rank-$(L_r, L_r, 1)$ BTD achieves a more general low-rank structure compared to CPD while preserving uniqueness under relatively mild conditions [37].

12.5 Applications of tensors in neuroimaging

This section gives an overview of successful tensor-based analysis techniques in neuroimaging studies. It will become evident that tensor structures and decompositions can be useful at any given stage of the data processing pipeline. First, various

preprocessing problems are discussed. Images may be corrupted; therefore, filling in missing data (Section 12.5.1), denoising, and artifact removal may be necessary. Furthermore, dimensionality reduction may be applied in order to reduce the computational complexity of subsequent processing steps (Section 12.5.2). Once the images are conditioned, image segmentation (Section 12.5.3) may be applied in order to select areas of interest (e.g., a tumor) or reject areas of no interest (e.g., skull or ventricles). When multiple images need to be compared or processed together – such as in a longitudinal study, tracking the evolution of a patient using repeated images over time—these need to be coregistered first (Section 12.5.4).

While the preprocessing steps mentioned above are important both in structural and functional imaging, certain data processing problems are specific for functional imaging. Functional neuroimaging techniques record a time series at different spatial locations, and they typically capture various sources of brain and other physiological activity, as well as noise. Source separation (Section 12.5.5) techniques are crucial to disentangle the activity of these sources. In many applications the ultimate goal is to recognize a specific activity of interest (e.g., the occurrence of an epileptic seizure) and to localize it, as discussed in Section 12.5.6. In other contexts, understanding the global behavior of the brain can be of interest. Structural connectivity analysis aims to establish how the anatomically distinct brain regions are physically interconnected. Functional connectivity analysis, on the other hand, explores the statistical interdependence between the activity time courses of different anatomical regions (Section 12.5.7). These interdependencies may provide insight into the intrinsic organization of the brain activity and how distinct brain regions cooperate. Functional connectivity may be studied in the resting state or examined during task execution. In the latter case—in a well-controlled experiment—the known time course of the task paradigm can be used as a model for the expected brain activity. Then, regression analysis (Section 12.5.8) can reveal if the model explains the observed brain activity, to what extent, and in which brain regions exactly. The ultimate goal of (clinical) neuroimaging is assisting diagnosis: distinguishing between healthy and pathological images or activity. To this end, Section 12.5.9 introduces tensor techniques for feature extraction and classification.

Besides the listed applications, tensors are excessively used in data fusion to handle large-scale data acquired from different modalities. Particularly, fusion of EEG and fMRI has been very prevalent in neuroscience due to the high temporal resolution of the first and high spatial resolution of the latter. Therefore, tensor-based fusion methods of EEG and fMRI are investigated in detail separately in Chapter 11 (Coupled tensor decompositions for data fusion).

12.5.1 Filling in missing data

Estimation of missing data is essential in many signal and image processing applications arising from any kind of information loss or errors in data collection. For instance, in the concept of neural signals, a sensing component such as an electrode might become loose, the signal may become saturated due to large movements,

or data may be lost during transfer. These problems may lead to missing fibers or random missing entries throughout the tensor, respectively (Fig. 12.10). Tensor completion methods aim at filling such missing entries of incomplete tensors.

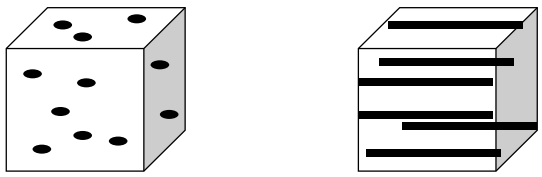

(a) (b)

FIGURE 12.10

An example tensor with (a) random missing entries and (b) missing channels [43].

The first application of tensor completion on neuroimaging data is proposed in [38]. The authors reformulate the CANDECOMP/PARAFAC (CP) model for EEG data as a weighted least-squares problem where only the known entries are modeled. The developed algorithm, named CP-weighted optimization (CP-WOPT), expresses the weighted CP formulation as

$$f_{\mathcal{W}}(\mathbf{U}^{(1)}, \mathbf{U}^{(2)}, \mathbf{U}^{(3)}) = \sum_{i=1}^{I}\sum_{j=1}^{J}\sum_{k=1}^{K}\left\{w_{ijk}\left(x_{ijk} - \sum_{r=1}^{R} u_{ir}^{(1)} u_{jr}^{(2)} u_{kr}^{(3)}\right)\right\}^2, \quad (12.12)$$

where $\mathcal{X}$ shows the EEG tensor with factor matrices $\mathbf{U}^{(1)}, \mathbf{U}^{(2)},$ and $\mathbf{U}^{(3)}$, i, j, and k denote the indices in the first, second, and third mode, respectively, of the corresponding tensor, and $\mathcal{W}$ is the weight tensor defined as

$$w_{ijk} = \begin{cases} 1 & \text{if } x_{ijk} \text{ is known,} \\ 0 & \text{if } x_{ijk} \text{ is missing.} \end{cases} \quad (12.13)$$

Finally, Eq. (12.12) is directly solved using first-order nonlinear optimization.

The authors test CP-WOPT on EEG data recorded during proprioceptive stimuli of the left and right hands of 14 subjects, making 28 measurement conditions in total. The constructed EEG tensor has three modes: *measurement condition*, *channel*, and *time-frequency*, which is obtained using continuous wavelet transform. Their results show that CP-WOPT can capture the underlying brain activity even when almost half of the electrodes are missing. Last but not least, CP-WOPT is noted to be much faster than its matrix- and tensor-based alternatives due to the fact that the missing entries are neglected in the cost function.

In CP-WOPT, the rank of the input tensor is assumed to be known, i.e., it has to be entered manually. In return, [39] states that a rising number of missing entries increases the chance of incorrect specification of the tensor rank, which results in deterioration of the performance of such tensor factorization schemes. Instead, the

authors propose to model the input tensor as a combination of the true latent tensor (generated by tensor factorization with a low CP rank), sparse outliers, and isotropic Gaussian noise (Fig. 12.11) and determine the rank of the latent tensor automatically by minimizing the dimensionality of the latent space. This minimization corresponds to column-wise sparsity of factor matrices in each mode. Thus, sparsity inducing priors are employed over all unknown parameters. This way, all parameters, including the CP rank, are determined automatically under a Bayesian framework. This method is known as Bayesian CP factorization (BCPF). BCPF is used to recover EEG data with missing entries and denoise noisy MRI data in [40].

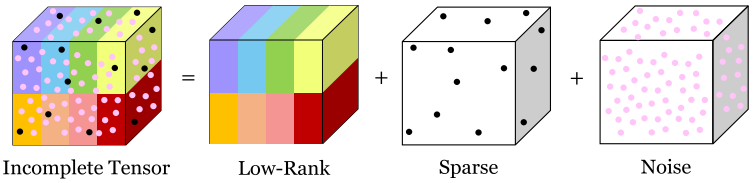

FIGURE 12.11

An incomplete tensor can be approximated as the summation of a low-rank tensor, sparse outliers, and isotropic noise [39].

In [41], the CP-WOPT is extended with rank regularization such that the proposed cost function becomes as follows:

$$\tilde{\mathcal{X}} = \arg\min_{\mathcal{Y}} \frac{1}{2}||(\mathcal{X} - \mathcal{Y}) * \mathcal{W}||_{\mathrm{F}}^2 + \lambda||\mathcal{Y}||_*, \tag{12.14}$$

where $\mathcal{W}$ is the binary weight tensor (Eq. (12.13)) that accounts for the missing entries, $||.||_*$ shows the nuclear norm operator, and $\lambda \geq 0$ is the rank controlling parameter. Simply put, Eq. (12.14) searches for a low-rank tensor $\tilde{\mathcal{X}}$ that has minimal distance to the original input tensor $\mathcal{X}$ over the available entries while achieving a low-rank structure via nuclear norm regularization.

The nuclear norm is used widely in optimization problems to search for low-rank solutions. In the case of a matrix, the nuclear norm becomes equivalent to the sum of its singular values, whereas the tensor nuclear norm is dependent on the choice of base field [42]. In [41], the authors define the nuclear norm of a third-order tensor $\mathcal{Y}$ based on CPD as

$$||\mathcal{Y}||_* = \min_{\{\mathbf{U}^{(1)},\mathbf{U}^{(2)},\mathbf{U}^{(3)}\}} \frac{1}{2}(||\mathbf{U}^{(1)}||_{\mathrm{F}}^2 + ||\mathbf{U}^{(2)}||_{\mathrm{F}}^2 + ||\mathbf{U}^{(3)}||_{\mathrm{F}}^2) \tag{12.15}$$

$$\text{subject to } \mathcal{Y} = \sum_{r=1}^{R} \mathbf{u}_r^{(1)} \circ \mathbf{u}_r^{(2)} \circ \mathbf{u}_r^{(3)}.$$

Expressing the CPD of $\mathcal{Y}$ with unit norm terms such that $\mathbf{a}_r = \mathbf{u}_r^{(1)}/||\mathbf{u}_r^{(1)}||$, $\mathbf{b}_r = \mathbf{u}_r^{(2)}/||\mathbf{u}_r^{(2)}||$, and $\mathbf{c}_r = \mathbf{u}_r^{(3)}/||\mathbf{u}_r^{(3)}||$ gives

$$\mathcal{Y} = \sum_{r=1}^{R} \gamma_r (\mathbf{a}_r \circ \mathbf{b}_r \circ \mathbf{c}_r) \tag{12.16}$$

with weights $\gamma_r = ||\mathbf{a}_r||\ ||\mathbf{b}_r||\ ||\mathbf{c}_r||$, $r = 1 \dots R$.

Finally, the completion problem can be reformulated as follows:

$$\tilde{\mathcal{X}} = \underset{\{\mathcal{Y}, \boldsymbol{\gamma}, \mathbf{a}_r, \mathbf{b}_r, \mathbf{c}_r\}}{\arg\min} \frac{1}{2}||(\mathcal{X} - \mathcal{Y}) * \mathcal{W}||_{\mathrm{F}}^2 + \frac{\lambda}{2}||\boldsymbol{\gamma}||_{2/3}^{2/3} \tag{12.17}$$

$$\text{subject to } \mathcal{Y} = \sum_{r=1}^{R} \gamma_r (\mathbf{a}_r \circ \mathbf{b}_r \circ \mathbf{c}_r).$$

The cost function provided above controls the tensor rank by inducing sparsity on the amplitudes of its rank-1 components. These priors are introduced on the tensor factors via a Bayesian framework. The proposed method is observed to outperform CP-WOPT when tested on corrupted 3D MR images.

In [43], the authors utilize tensor completion to fill in corrupted EEG data, which might originate from a high impedance between electrodes and scalp, motion, eye blinks, and so on. In other words, noisy measurements are treated as missing samples or unknowns, which are later inferred using a tensor approach. They model the EEG data as a tensor with modes *channel*, *time*, and *trial* and apply the following tensor completion algorithms: CP-WOPT, BCPF, 3D patch-based tensor completion [44], and high-accuracy low-rank tensor completion [45]. They evaluate the performance of the aforementioned completion methods by testing the classification accuracy of imagined movement in a BCI experiment with corruptions and missing channels. All four algorithms are reported to increase the classification accuracy when compared to the conventional approach of average interpolation across trials.

12.5.2 Denoising, artifact removal, and dimensionality reduction

Denoising, artifact removal, and dimensionality reduction algorithms are prerequisites to a majority of signal processing applications. An omnipresent tool in this context for matrix data is SVD, as it can capture signals and noise in different subspaces. Recognizing and rejecting the noise subspace achieves all above objectives. Therefore, multilinear extensions of SVD—MLSVD and CPD—are natural methods of choice in the case of tensor data. Indeed, many methods covered in this review intrinsically denoise or reduce the volume of input data by low-rank approximating them or by separating its components of interest from background data via various tensor decomposition techniques. Nevertheless, this section will be dedicated to algorithms that solely aim at denoising, artifact removal, or dimensionality reduction.

To begin with, different imaging modalities are prone to different types of artifacts. For instance, MRSI data are often corrupted by residual water, EEG signals

may be corrupted with ocular artifacts, while functional images are seriously distorted by head motion. These phenomena call for custom solutions, especially when it comes to identifying the noise subspace. Some examples are outlined below.

Residual water in MRSI accounts for a large variance in the data and should be suppressed to accurately assign brain metabolite signals [46]. In [47], the purification of MRS images from residual water is regarded as a source separation problem. To this end, first the MRSI input tensor $\boldsymbol{\mathcal{X}}$ is compressed via truncated MLSVD, leading to a core tensor $\boldsymbol{\mathcal{S}}$ and factor matrices $\mathbf{U}^{(n)}$ as given in Eq. (12.9). Truncated MLSVD is used to approximate $\boldsymbol{\mathcal{X}}$ as a smaller tensor $\boldsymbol{\mathcal{S}}$, whose size R_n is smaller than the actual column rank of $\boldsymbol{\mathcal{X}}_{(n)}$ along one or more modes (n) [28]. Next, CPD is applied on the compressed core tensor $\boldsymbol{\mathcal{S}}$. Finally, the components whose resonance frequencies (as given by MRSI) are outside the region of interest are marked as water components. As expected, such a twofold procedure with MLSVD and CPD is observed to be particularly beneficial when the input tensor is large.

EEG signals can be seriously distorted by ocular artifacts, i.e., large changes in the electric field caused by the movement of the eyeball which acts as a dipole [48]. Assuming that the ocular artifacts and brain activity are independent, [49] proposes a tensor decomposition scheme to automatically remove these artifacts. As the cumulants of such independent sources lead to a superdiagonal tensor [50], [49] diagonalizes the fourth-order EEG cumulant tensor through CPD. The extracted components are thresholded in terms of their kurtosis values in order to automatically identify the ocular artifacts to be removed.

Like many neuroimaging modalities, fNIRS data are prone to artifacts caused by relative motion between the scalp and fNIRS optical fibers [51]. For removal of motion artifacts, [52,53] apply CPD to 3D fNIRS tensors with modes *space*, *time*, and *wavelength* (accounting for the different wavelengths used in fNIRS for absorption of both oxygenated and deoxygenated hemoglobin). Similarly, [54] uses CPD on 3D water diffusion maps of DT images in order to extract only the components of interest that correspond to major fiber orientations.

The approaches described above consider the existence of undesired artifact components in data, which can be even more powerful than the activities of interest [46]. Therefore, after decomposing the input tensor into its components, some of these components (that point to artifacts) are removed either manually or automatically. However, tensor decomposition techniques can also be used to denoise an input tensor by finding a low-rank approximation of it, without explicitly rejecting a portion of the extracted components. For example, [55] proposes a method to jointly reconstruct and denoise PET images via low-rank approximating a PET feature tensor $\boldsymbol{\mathcal{X}}$ using tensor nuclear norm regularization:

$$\tilde{\boldsymbol{\mathcal{X}}} = \arg\min_{\boldsymbol{\mathcal{Y}}} \frac{1}{2}||(\boldsymbol{\mathcal{X}} - \boldsymbol{\mathcal{Y}})||_{\mathrm{F}}^2 + \lambda||\boldsymbol{\mathcal{Y}}||_*, \tag{12.18}$$

where $\boldsymbol{\mathcal{Y}}$ can be decomposed using tensor SVD (Eq. (12.10)) and λ controls the nuclear norm regularization. The authors use an intuitive approach [56] based on

tensor SVD to define the tensor nuclear norm:

$$||\mathcal{Y}||_* = \sum_{r=1}^{R} s_{rr1}, \tag{12.19}$$

where R defines the rank. This way, a closed-form solution is obtained for reconstruction. The proposed scheme is observed to accomplish more than mere denoising of PET data, providing enhancement to the reconstructed images by intensifying structural information.

Moreover, tensor decomposition methods can be used to reduce the dimensionality of input data without losing valuable information. Considering the remarkable performances achieved by deep learning methods in various signal processing applications over the past decade, dimensionality reduction becomes even more critical due to the curse of dimensionality of input training data. The curse of dimensionality refers to the fact that an increase in the dimensionality of input data will demand an exponentially growing storage space.

Particularly in medical image processing, convolutional neural networks (CNNs) have gained significant attention, which have the advantage of combining feature extraction and classification steps. To reduce the dimensionality of CNN inputs, [57] proposes a CPD-based framework for an input EEG tensor $\mathcal{X}$ with modes *time*, *frequency*, and *channel*.

First, CPD is applied on the input tensor producing the factor matrices $\mathbf{U}^{(1)}$, $\mathbf{U}^{(2)}$, and $\mathbf{U}^{(3)}$ along the modes *time*, *frequency*, and *channel*, respectively. In order to reduce the number of channels by only selecting the ones that are of interest, a projection matrix is defined as $\mathbf{P} = ((\mathbf{U}^{(3)})^{\mathrm{T}}\mathbf{U}^{(3)})^{-1}(\mathbf{U}^{(3)})^{\mathrm{T}}$. The new low-rank representation $\tilde{\mathcal{X}}$ of $\mathcal{X}$ is found by $\tilde{\mathcal{X}} = \mathcal{X} \times_3 \mathbf{P}$, which converts the original channel slices into superslices. The number of superslices is equal to the rank of CPD. Employing superslices does not only reduce the dimension of CNN training inputs, but also handles the artifacts and redundancies of the EEG signals. The proposed method is tested with various time-frequency transformations and CNN parameters. Compared to 1D and 2D state-of-the-art dimensionality reduction techniques including PCA, the proposed tensor-based framework is observed to perform better in terms of classification accuracy for seizure detection.

In parallel to the increasing interest towards dimensionality reduction methods that keep out the redundant parts of acquired data, a theory known as compressed sensing (CS) has emerged. Most neural signals exhibit a sparse representation naturally or in another domain. Using such sparse representations, CS techniques aim at directly sensing data in a compressed form. Conventionally, 1D or 2D sparsity bases are utilized to solve even higher-order problems. To make use of and preserve the high-dimensional structure in CS applications, [58] proposes MLSVD as a tensor sparsifying transform for 3D MRI data. More specifically, the authors directly apply MLSVD to the inverse Fourier transform of the zero-filled undersampled k-space measurements ($\mathcal{X}$) as in Eq. (12.9). The factor matrices $\mathbf{U}^{(n)}, n = 1, 2, ...N$, give the sparsity bases and are obtained by applying matrix SVD to the mode-n unfolding matrices $\mathbf{X}_{(n)}, n = 1, 2, ...N$. MLSVD leads to a sparse core tensor $\mathcal{S}$ due to

the all-orthogonality and ordering conditions applied to it, which guarantee that most of the energy of the core tensor lies around one vertex. The proposed approach is reported to improve image reconstruction quality when compared to 1D/2D sparsifying transforms.

12.5.3 Segmentation

Segmentation, as opposed to the preprocessing steps discussed so far, is specific for images rather than signals. The purpose of segmentation may be to discard nonbrain tissue from the image (skull, ventricles, etc.) or to partition the image of the brain into smaller meaningful regions. This can be achieved in a supervised or an unsupervised manner, i.e., with or without known labels. We will begin our overview with the latter.

For differentiation of tumor, necrotic, and normal brain tissue types, a nonnegative CPD (NCPD)-based segmentation from MRSI and multiparametric MRI (MP-MRI) data is proposed in [59] and [60] respectively. For MRSI data, a feature vector $\mathbf{x}$ is calculated for each voxel based on their spectra. For MP-MRI data, $\mathbf{x}$ at each voxel is constructed in a way that highlights different information brought from different modalities, namely MRI, PWI, DWI, and MRSI. By stacking the matrices $\mathbf{x}\mathbf{x}^{\mathrm{T}}$ for all voxels, a tensor $\mathcal{X}$ is obtained. Next, $\mathcal{X}$ is decomposed into R sources using NCPD. It should be mentioned that imposing constraints on factor matrices, such as the nonnegativity constraint here, can help to relax the uniqueness condition, reduce the computational cost, enhance robustness against noise, and increase the interpretability of the results [61]. In MP-MRI data, R is set manually whereas in MRSI data, R is automatically determined as follows. First, a data matrix is constructed by concatenating the spectra of each voxel and the covariance of the data matrix is estimated. Then, the eigenvalues of the spectra covariance matrix are calculated. Finally, R is estimated as the minimum number of eigenvalues whose cumulative sum is greater than 99% of the sum of all eigenvalues. The results on both imaging types show that NCPD is better at separating tumor tissue compared to matrix-based decompositions.

Although the approaches described above can successfully segment the images, the found segments still lack a label, for which a supervised classification approach is required. To this end, [62] proposes a two-stage fully automated superpixel-wise tumor tissue segmentation algorithm for MP-MRI data. The algorithm employs a random forest classifier with truncated MLSVD-based feature extraction, which first identifies the whole tumor and then divides it into its subregions. In [63], a CNN architecture with MLSVD-based low-rank regularization on the convolutional layers is proposed to label MRSI voxels as "tumor," "bad quality," or "normal." MLSVD is observed to give faster results (as the number of computations is lowered) without causing a significant change in the performance of CNN.

Medical images are volumetric, and hence many neural network models have also embraced 3D CNN architectures for their segmentation. These models include the 3D extension of the U-Net, which is one of the most prominent medical image

segmentation networks so far [64]. U-Net takes its name from its architecture, which indeed looks similar to the letter U. The first half of the network is the contracting part, where the input image is encoded into feature maps at various levels for classification. The second half is the expanding part which up-samples the feature maps to be localized at the input pixel space [65]. The 3D U-Net model replaces the 2D operations in the original model with their 3D versions. In [66], the authors propose adding volumetric feature recalibration (VFR) layers to the 3D U-Net architecture as shown in Fig. 12.12. A VFR layer takes an input feature tensor and low-rank regularizes it to a rank-1 tensor using CPD. Such regularization forces only the most critical patterns within the feature tensor to be captured and leads to smooth spatial changes in the segmented tissues across adjacent slices, which is in line with the anatomical organization of the brain. The proposed model is used for segmentation of major brain tissues—namely the white matter, gray matter, and cerebrospinal fluid—from MRI data, and currently ranks first in the MRBrainS13 Challenge [67].

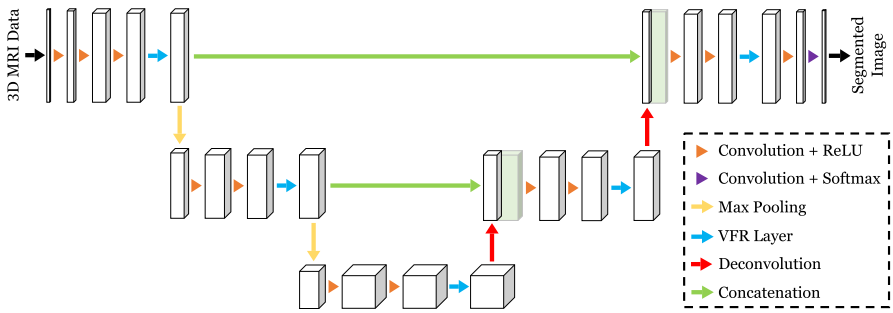

FIGURE 12.12

The 3D U-net architecture with VFR layers proposed in [66].

12.5.4 Registration and longitudinal analysis

Image registration is defined as the process of geometrically aligning two or more images and allows comparison of datasets across subjects, conditions, modalities, or time. Thus, it is a prerequisite to numerous neuroimaging applications [68]. For instance, registration of a subject and a control brain helps revealing abnormal regions in the subject brain. As a particular case of neurological image registration, longitudinal studies explore the changes in a subject's brain across his/her life span and show the evolution of the structure or function of progressive diseases [69].

Tensor-based morphometry (TBM) is a tensor solution to track differences in two brain images by constructing a Jacobian change map at the voxel level that is computed by nonlinearly registering a scan of interest to a baseline scan. Mathematically, for each voxel (x, y, z), a displacement vector $\mathbf{d} = (d_x, d_y, d_z)$ is found between a 3D

study scan $\mathcal{S}$ and a 3D template scan $\mathcal{T}$ such that $t_{(x-d_x)(y-d_y)(z-d_z)} = s_{xyz}$. Then, the Jacobian matrix of the deformation field at (x, y, z) is calculated as [70]

$$\mathbf{J}(x, y, z) = \begin{pmatrix} \partial(x - d_x)/\partial x & \partial(x - d_x)/\partial y & \partial(x - d_x)/\partial z \\ \partial(y - d_y)/\partial x & \partial(y - d_y)/\partial y & \partial(y - d_y)/\partial z \\ \partial(z - d_z)/\partial x & \partial(z - d_z)/\partial y & \partial(z - d_z)/\partial z \end{pmatrix}. \tag{12.20}$$

The determinant of Eq. (12.20) gives the Jacobian at (x, y, z). For instance, a Jacobian value of 0.9 or 1.1 corresponds to a 10% tissue loss or a 10% tissue gain, respectively, in the local volume [71]. The 3D Jacobian change map is obtained by calculating the Jacobian for all voxels. An illustration of longitudinal analysis by TBM is given in Fig. 12.13.

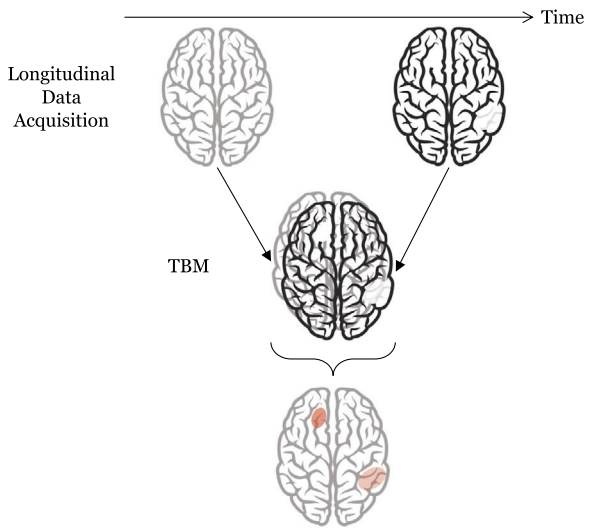

FIGURE 12.13

Illustration of TBM for longitudinal analysis. The template brain is a prior scan of the same subject to quantify the voxel-level differences that have occurred in time. These differences are marked by TBM based on the Jacobian of the deformation field.

In [72], the authors apply TBM to 3D MR images acquired 1 year apart from three groups of subjects: patients with Alzheimer's disease (AD), patients with mild cognitive impairment (MCI), and a control group of healthy patients. Consistent with prior studies, the authors report a widespread cerebral atrophy in patients with AD and a more restricted atrophic pattern in patients with MCI.

In [71], it is argued that using logarithmic transformation on the Jacobian values is crucial while evaluating the volumetric differences as it symmetrizes the Jacobian distribution by assigning equal probabilities to tissue gains and losses that are reciprocals of each other. The authors validate their claim on sequential MRI scans of a patient diagnosed with semantic dementia.

TBM is used to demonstrate HIV-induced brain damage from T1-weighted MR images in [73]. A 3D profile of brain tissue reduction is constructed by calculating the ratio of the mean Jacobian in HIV patients to the mean Jacobian in control subjects at each voxel. In addition, using the Mann–Whitney U test, which evaluates the randomness of the voxel-wise difference between the mean log-Jacobian in HIV patients and the control group, a significance map is constructed (high significance corresponds to the differences being true, i.e., not random). Their results show that the greatest tissue loss occurs in primary and association sensorimotor areas.

Anatomical differences in the brains of HIV patients are also examined in [70] from their MRI scans. The authors also compare using multivariate statistics of the Jacobian matrix to the conventional approach of using its univariate statistics (such as its determinant). The proposed multivariate method (based on manifold testing) is observed to more extensively reveal the atrophy of gray and white matter caused by HIV.

TBM analysis with log-transformed Jacobian maps is used to identify regional differences in brain volume based on prenatal alcohol exposure in [74]. To this end, the T1-weighted MR scan acquired from each subject is compared to an average anatomical template obtained from the control group. Furthermore, ICA is applied on the log-Jacobian maps to better identify brain tissue deformations. The deformations obtained after ICA are observed to be useful indicators of the presence and extent of prenatal alcohol exposure.

Finally, it is also possible to reflect on longitudinal analysis from a tensor decomposition point of view. In [75], a DTI tensor with modes *fiber*, *longitudinal features*, and *cross-section* is constructed and factorized using CPD. In the end, pathological longitudinal changes appearing along white matter fibers caused by multiple sclerosis are detected.

12.5.5 Source separation

Blind source separation (BSS) is the unmixing of original source signals from their intermixed observations. In general, tensor decomposition methods aim at factorizing a data tensor into several components. However, in many cases, the defined objective requires focusing on only one of those components, such as the seizure component, whereas the others are simply regarded as background noise [90]. We discuss the use of tensor decompositions for denoising in Section 12.5.2. Similarly, even when the objective is to compare the content of data along various modes across different experimental conditions, such as during the resting state and during a mental task, the data belonging to these conditions can be collected at different times and analyzed individually [89], without the need for source separation. This section will be dedicated to algorithms which consider *multiple* sources of interest that are active during the experiment time.

BSS is divided into the following two main groups: instantaneous (Eq. (12.21)) and convolutive (Eq. (12.22)), i.e.,

$$x_i(t) = \sum_{r=1}^{R} a_{ir} s_r(t) + e_i(t), \tag{12.21}$$

$$x_i(t) = \sum_{r=1}^{R} \sum_{l=0}^{L} h_{ir}(l) s_r(t-l) + e_i(t), \tag{12.22}$$

where $x_i(t)$, $s_r(t)$, and $e_i(t)$ are measurement, source, and noise signals, respectively, and R is the number of sources. The linear mixing coefficients a_{ir} of the instantaneous case are generalized by incorporating memory to the system in the form of convolutive mixing filters $h_{ir}(l)$ of length L in the convolutive case.

Tensor decompositions are common and intuitive tools for solving the BSS problem [76]. Indeed, note that Eq. (12.21) can be written in the form of

$$\mathbf{X} = \sum_{r=1}^{R} \mathbf{a}_r \circ \mathbf{s}_r + \mathbf{E}, \tag{12.23}$$

where the measurement matrix $\mathbf{X}$ holds all measurement vectors along its rows and the mixing vector $\mathbf{a}_r$ holds all a_{ir} coefficients. As described in Section 12.3, neuroimaging data often take the form of a tensor, either when a number of measurements are made in multiple domains, such as at multiple locations (channels), in multiple patients, in multiple conditions, etc., or via the tensorization of a measurement matrix. Then, the above equation becomes

$$\boldsymbol{\mathcal{X}} = \sum_{r=1}^{R} \mathbf{a}_r \circ \mathbf{b}_r \circ \ldots \circ \mathbf{s}_r + \boldsymbol{\mathcal{E}}, \tag{12.24}$$

which is analogous to the definition of CPD in Eq. (12.7). Then, the result of CPD can be interpreted as follows. Each of the R components $\mathbf{a}_r \circ \mathbf{b}_r \circ \ldots \circ \mathbf{s}_r$ corresponds to an individual source, each of the signatures $\mathbf{a}_r, \mathbf{b}_r, \ldots$ describes a certain property of the source, such as its variability in space, among patients, etc., and the temporal signature $\mathbf{s}_r$ describes the time course of the source.

For example, [77] uses CPD to localize several epileptogenic sources from EEG measurements, where these sources are simultaneously active at different brain regions. The EEG data are tensorized as a 3D *space*, *time*, and *wave* vector (STWV), regarding which more details will follow in Section 12.5.6.1. The spatial signatures of the extracted CPD components are observed to be pointing to the epileptogenic sites as confirmed directly by intracerebral stereotactic EEG recordings. An illustration of the presented methodology is provided in Fig. 12.14.

Despite the fact that neuroimaging data are often inherently multidimensional, matrix-based methods are well established and widely used. ICA, for example, is widely used for matricized fMRI data where the spatial modes are unfolded into a single long voxel mode. As a result, the spatial structure of the data is lost. In order to retain the spatial structure, [78] represents the fMRI data as a 4D tensor with modes

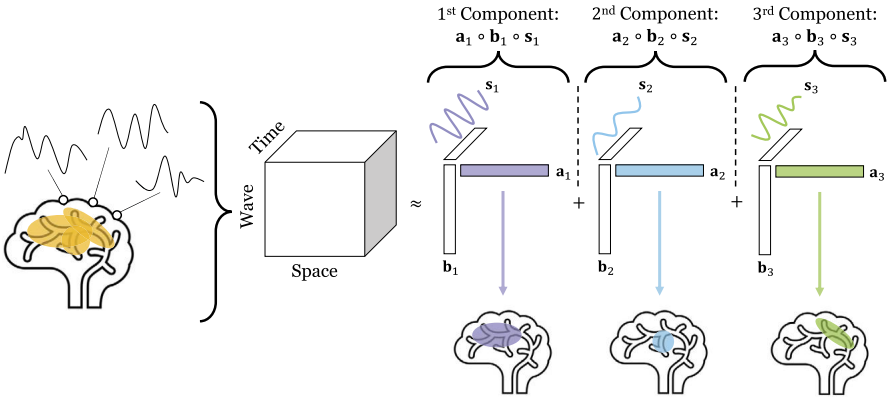

FIGURE 12.14

An illustration of CPD-based source separation with three sources. This approach is utilized in [77], where the collected EEG data consisting of mixed observations of the underlying sources are tensorized according to the STWV format (the spatial and temporal signals of this illustration are arbitrary and provided only for visualization). Each extracted component is defined by the outer product of its signatures and stands for one site of epileptic activity.

depth-length $\times$ *width* $\times$ *time* $\times$ *subject*. Then, various tensor-based instantaneous BSS techniques are applied, which are explained below.

The standard CPD modeling assumes the same (up to a scaling) underlying signal sources (spatial maps and time courses) for all subjects. However, empirical studies show that the impulse responses, known as the hemodynamic response functions (HRFs), leading to the blood signals acquired with fMRI change across subjects and brain regions. PARAFAC2 relaxes the strict multilinear assumption of CPD by allowing variation along one mode, i.e., subjects, as shown in Fig. 12.15.

Nevertheless, similar to CPD, PARAFAC2 still holds the rank-1 assumption, which is unrealistic for the spatial signatures of true brain sources. Consequently, the authors propose a PARAFAC2-like BTD model to achieve nonstrict multilinear modeling while incorporating higher-order components. When applying BTD/BTD2, the spatial signature of each source is assumed to be low-rank and the temporal signature is assumed to be rank-1. Different from BTD, BTD2 offers different time courses for each subject. Both in simulations and augmented datasets, nonmultilinear methods (BTD2 and PARAFAC2) are shown to be more suitable for BSS of fMRI data. Furthermore, BTD2 is observed to be significantly more robust to noise compared to PARAFAC2 at the cost of increasing computational complexity. Note that the assumption of independent sources—which has proved to be powerful in the fMRI literature—was not made in this study.

A second-order tensor-based convolutive ICA method is utilized to jointly address convolutive source separation and blind deconvolution of fUS data in [81]. In the proposed signal model (Eq. (12.22)), the hemodynamic response signals acquired with fUS correspond to the measurement signals $x_i(t)$, whereas the source signals $s_r(t)$

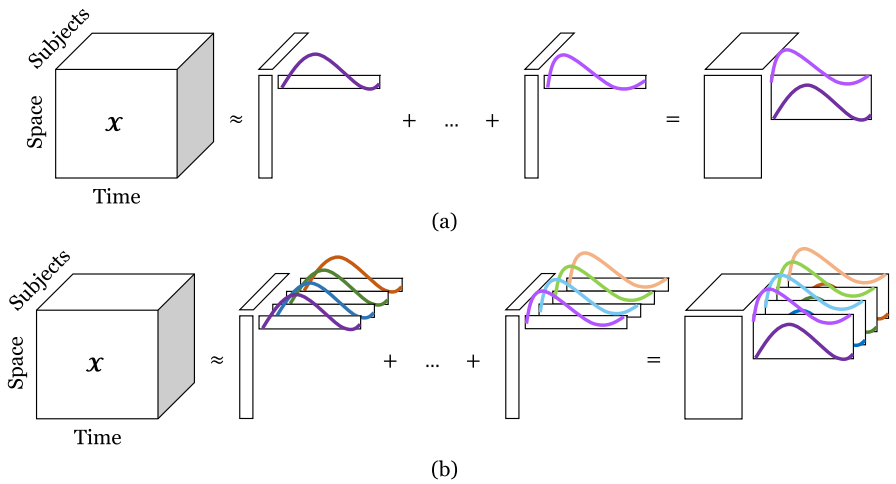

FIGURE 12.15

(a) CPD and (b) PARAFAC2 over an example space-time-subject tensor [79]. CPD can accommodate different temporal and spatial signature pairs for different neural components, but these are assumed to be the same for each subject up to a scaling factor. On the other hand, PARAFAC2 offers flexible temporal representations (which is necessary to model the HRF variability) across subjects.

represent the events that trigger these responses in the brain. Finally, the convolutive mixing filters $h_{ir}(l)$ stand for the HRFs. It is shown that if the sources are assumed to be uncorrelated, the tensor consisting of lagged measurement autocorrelation matrices can be factorized with a block-diagonal core tensor with inner Toeplitz blocks, which in the end leads to a BTD with constant rank terms [80].

The proposed approach has three main advantages. The first one is that the HRFs can be estimated differently based on the measurement and source index, which accounts for the HRF variability across brain regions and events, respectively. The second one is that the model offers a multiple input–multiple output solution, which is suitable for representing the complex interactions leading to hemodynamic activity of brain voxels. Last but not least, the unknown HRFs and neural stimuli can be identified simultaneously via BTD.

The convenience of tensor-based solutions to BSS problems is investigated in a wide range of neural signal processing applications in [82]. Several methods including tensor-based singular spectrum analysis and complex PARAFAC2 are employed for analysis of both single and multichannel signals. For more information on the topic, we refer the reader to the abovementioned paper.

In the following section, we discuss an important application of tensor-based BSS in neuroimaging. More specifically, careful interpretation of the signatures resulting from appropriate tensor decompositions can lead to successful activity recognition and source localization.

12.5.6 Activity recognition and source localization

Functional neuroimaging tools collect signals (directly or indirectly) from millions of neurons, which communicate in time and space through short bursts of oscillations. The goal of activity recognition is to establish if and when a certain neural process takes place, such as a particular stage of cognitive processing or a pathological event (e.g., an epileptic spike). Subsequently, one may aim to localize those neuronal populations which are involved in the activity of interest.

Brain data have conventionally been described by a matrix, with time courses or spectral information along one mode and information from different channels organized along the other mode. The data are later decomposed using a matrix factorization technique, such as PCA [83] or ICA [84]. Finally, each component is represented by two vectors (time *or* frequency and space) which are often called signatures. The assumption of orthogonality (PCA) or independence (ICA) ensures a unique solution. If the assumption is plausible, one can be confident that the components correspond to the actual sources and the signatures describe the true physical properties of the sources. In turn, these signatures allow to recognize the activity of interest. As described in the previous section, this idea can be extended to multilinear analysis using CPD, with the advantage that it can describe the data in more than two domains (i.e., time *and* frequency and space), and leads to a unique solution without hard constraints as in the matrix case [85].

CPD has been developed in 1970 in psychometrics by two independent studies that extend factor analysis to multiway signals, one of which has defined the process as parallel factor analysis, whereas the other defined it as canonical decomposition [86]. Approximately a decade later, [87] has practiced, to the best of our knowledge, one of the very first uses of CPD (and multidimensional analysis) on brain signals. In this study, the authors report differential hemispheric activity with positive emotional tasks being associated to right temporal activity after applying CPD on an EEG tensor with *channel* $\times$ *time* $\times$ *subject* modes. CPD was later used by [88] under the name of topographic component analysis for processing of event-related potentials (ERPs) described by the same modes and supported with biophysical considerations.

Another common three-way representation of EEG data combining *spatial*, *spectral*, and *temporal* modes is proposed initially in [89]. The spectral information is obtained using wavelet transform, which is often chosen for its optimal time-frequency resolution by resolving high-frequency components within small time windows and low-frequency components in larger time windows [90]. After applying CPD on the 3D EEG tensors with space-time-frequency (STF) modes, in line with previous findings, frontal theta components and occipital alpha components were identified during separate analysis of a mental arithmetic task and the resting condition, respectively.

This work was extended by addition of *condition* and *subject* modes [91]. This way, the differences in STF modes can be identified based on subjects and conditions (object or nonobject drawings are presented to subjects) through a single CPD computation. For instance, the "object condition" is observed to be more active in the occipital region at the lower gamma band than the "nonobject" condition. In [92], the same 5D tensorization (except with Hanning windowed fast Fourier transform

for construction of the spectral mode) is used to analyze transcranial magnetic simulation (TMS)-induced EEG responses, known as TMS-evoked potentials (TEPs). Using CPD, TEPs are analyzed under four conditions as predrug and postdrug status of two different drug types. The results unveil three unique signatures along the space and frequency modes as frontal-sensorimotor beta, posterior alpha, and theta (whose location is observed to depend on the site of stimulation) components. Furthermore, the inter-subject variability is characterized by the fourth mode, whereas on the fifth mode drug effects are revealed, such as an observed reduction in postconditions of both drugs for all components.

CPD of evoked EEG signals acquired from healthy subjects and patients with chronic pain, each condition represented by an STF tensor, was also used to highlight differences across modes based on the subject's health condition [93]. More specifically, the active neural response of chronic pain patients was spotted around the frontal region with lower frequency values compared to the control group, whose active location is detected around the central region.

On fNIRS data, CPD is applied to identify the temporal and spatial characteristics of a verbal task in [52]. For this purpose, a 3D tensor with modes *space*, *time*, and *wavelength* was constructed. The wavelength mode entails two bands in the near-infrared spectrum for extraction of the hemodynamic response based on oxygenation of hemoglobin. The results show that CPD is capable of both motion-artifact removal and identification of task-related activity, which is confirmed with commonly used approaches in the fNIRS literature such as the general linear model. CPD of fNIRS data (*time* $\times$ *channel* $\times$ *frequency* $\times$ *subject*) is also used to investigate differences in spatial, temporal, and spectral patterns of infant brain reactions to human and mechanical hands [94].

Detection and localization algorithms focusing on epileptic seizures will be investigated separately considering the significance of and the large amount of work dedicated to epilepsy, which is one of the most common neurological disorders, influencing around 70 million people worldwide [95]. Epilepsy is characterized by recurrent seizures which take place due to excessive electrical discharges in a group of brain cells which are observed as rhythmic patterns in brain recordings. Seizures can start in one part of the brain and continue to spread throughout the brain, affecting more parts of the body unless prevented, as shown in Fig. 12.16. These seizures can potentially be cured by surgically removing the seizure focus, if it is accurately localized, or by blocking the spread of the seizures using medication or stimulation if the onset of the seizure is detected early on [97]. Neuroimaging tools combined with signal processing techniques can be helpful in both treatment approaches.

12.5.6.1 Seizure localization

Seizure localization aims to identify the seizure onset zone in the brain. In other words, the main interest is on the spatial content of seizure component(s).

Applying CPD on EEG data for seizure localization is proposed in [90] by constructing a 3D STF tensor with wavelet transform defining the spectrum array. The optimal rank value for CPD is determined as two by applying the core consistency

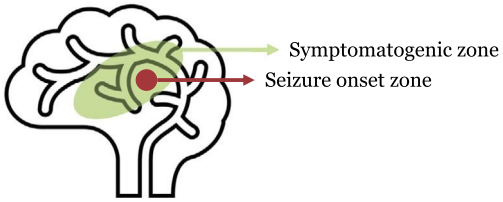

FIGURE 12.16

Epileptic activity zones. The seizures start in the seizure onset zone and might spread to adjacent areas (symptomatogenic zone) [96].

diagnostic [98]. In order to identify which of the two components arises from epileptic activity, both components are ordered according to their contribution in the spatial mode in terms of their variance, and the component with the highest contribution is classified as the epileptic component. The authors claim the following for this selection. Seizure activity has more stable spectral and spatial signatures compared to background EEG, which is expected to be more random. Therefore, CPD will be relatively insensitive to background EEG, and model the dominant, i.e., epileptic, activity. Although the spatial signature of the epileptic component is assumed to correspond to the spatial distribution of epileptic activity, only the electrodes showing a potential above a predefined threshold are used to define the exact focus of the seizure. Furthermore, it is observed that the maximum frequency in the spectral content of the epileptic component corresponds to the frequency of the rhythmic seizure.

A Tucker decomposition approach for seizure localization on EEG data is proposed in [99]. Tucker decomposition on STF tensors is compared to two-way decomposition methods such as SVD and PCA constructed with either *space* $\times$ *time* or *space* $\times$ *frequency* modes. The results obtained show that multiway analysis achieves more precise localization compared to two-way analyses. Nevertheless, the authors state that it is much more difficult to interpret the resulting components from Tucker decomposition compared to those from CPD. This is due to the fact that CPD extracts multilinear components, where each component is described by the interactions of exactly one signature from each mode, which directly match the properties of the given component. However, Tucker decomposition employs a core tensor that allows the interaction of multiple signatures from each mode (Section 12.4). Therefore, the individual signatures cannot be interpreted alone.

Overall, CPD provides a more restricted and simpler model compared to Tucker decomposition for seizure localization [100]. However, EEG data recorded during a seizure are often contaminated with eye blinks, eye movements, and muscle artifacts, which might interfere with the expected dominance of epileptic activity over background EEG in the case artifacts account for most of the variation. Therefore, [100] proposes combining CPD of STF tensors of EEG data with an artifact removal stage through multilinear subspace analysis. The optimal rank value for CPD is determined via the core consistency diagnostic. Although the decomposed terms are labeled as

artifact or seizure using clinical feedback from neurologists, when the spectral signatures of components were compared, the authors noticed that most artifacts lie in a low-frequency band whereas high-frequency content is present for epileptic activity, which can be a potential lead for automating the component selection process. For artifact removal, the authors suggest using Tucker decomposition which returns factor matrices along STF modes. Based on visual inspection of the components in the spatial mode, the artifact components are determined. The original tensor is then projected onto the null space determined by the artifact components. The resulting artifact-free tensor is then provided as input to CPD.

Seizure localization on neonatal EEG data is investigated under two different seizure types in [101], namely oscillatory and spike-train type seizures. For oscillatory seizures, CPD is applied to the STF tensor using the core consistency diagnostic as in [90] whereas for spike-train type seizures, the 3D EEG tensor is constructed differently. More specifically, spikes are detected [102] and segmented from each channel and placed into a tensor. In other words, the constructed tensor at each slice has the segmented data from all channels where the segments are constructed whenever a spike is detected. This tensor is decomposed into its signatures using a rank-1 CPD as the proposed tensorization method only captures seizure data (Fig. 12.17). Consequently, the resulting spatial signature corresponds to the spatial distribution of the seizure.

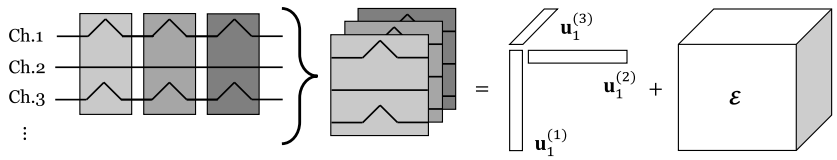

FIGURE 12.17

CPD-based approach for spike-train seizure localization proposed in [101] where $\mathcal{E}$ shows the residual tensor. As the input tensor is constructed using only seizure segments, a rank-1 CPD is applied to obtain the seizure component.

CPD expresses the STF EEG tensor into a sum of rank-1 tensors, which means every extracted term is defined by the combination of exactly one spatial, temporal, and spectral signature. Therefore, stating that in cases where the seizure pattern is nonstationary such a trilinear signal model will be insufficient, [103] proposes to use BTD for seizure localization with EEG. Decomposition into rank-$(L_r, L_r, 1)$ terms facilitates the extraction of sources that are rather fixed along one mode but vary in others, such as sources with a constant spectral structure that spatially spread over time or sources which evolve in frequency but are spatially constrained. BTD is also useful in combination with a Hankel expansion (instead of time-frequency expansion) of the data, based on the assumption that EEG signals can be modeled as a sum of exponentially damped sinusoids. The Hankel matrix of a time series has a low rank depending on the number of underlying sinusoids. Assuming that the multichannel EEG records the linear mixture of such sources, the data admits a rank-$(L_r, L_r, 1)$

model indeed. The authors show three scenarios in which BTD is more successful than CPD in localizing the seizure according to clinical assessment: a seizure with severe eye artifacts, with evolving frequency, and with varying locations. Nevertheless, the performance of BTD is observed to depend heavily on the appropriate selection of the number of extracted components (R) and the rank of the factor matrices (L_r).

CPD is applied to STWV tensors for seizure localization on EEG data in [77]. A wave vector corresponds to a local spatial Fourier transform within a certain region on the scalp defined by a spherical window function. The STWV modeling is shown to yield better results compared to STF, especially with correlated sources, i.e., when similar epileptic spikes spread in multiple regions with short time delays in between. In addition, the authors provide a theoretical explanation on the conditions explaining the functioning and performance of trilinear STF and STWV analyses such as the source strengths and source correlations in time and space.

12.5.6.2 Seizure recognition

Seizure recognition refers to determining the time intervals in which a seizure takes place (detection) or there are indications that a seizure might be approaching (prediction). While the former can replace a manual seizure diary, the latter especially can allow triggering of warning devices beforehand and prevent serious injury.

One way for seizure detection is dividing the brain data into time segments (epochs), extract features from each epoch, and classify the features as "seizure" or "nonseizure." In [104], an EEG tensor for each epoch is constructed using wavelet or Hilbert–Huang transform with STF modes. Features from each epoch are extracted from the signatures obtained with CPD and BTD of the corresponding tensor. In order to determine the optimal rank value for decomposition, MLSVD is utilized. The MLSVD core is truncated until the singular values represent more than 95% of the data variance. Low-multilinear rank approximation is initialized with the truncated MLSVD core, which finds the multilinear rank that best approximates the tensor in the least-squares sense. Several classifiers are used to label the epoch features, namely K-nearest neighbor, radial basis support vector machine (SVMRB) and linear discriminant analysis. The classifiers are trained with one seizure segment while the remaining data are used for testing. The block diagram of the proposed method is provided in Fig. 12.18. The best results are obtained when spatial signatures are used as features and the SVMRB as classifier.

Alternatively, features can be included inside the tensor. One such feature tensor is proposed in [105] with modes *time epoch*, *feature*, and *channel*, where the features are created in time and frequency modes in a way to create distinction between seizure and nonseizure periods of EEG data. The tensor is regressed to seizure and nonseizure classes using multilinear partial least-squares.

A deep learning solution to seizure detection has been proposed in [57] and discussed in detail in Section 12.5.2. In summary, the authors introduce a CPD-based dimensionality reduction stage to obtain a low-rank approximation of the original EEG tensor to be given as input to a CNN.

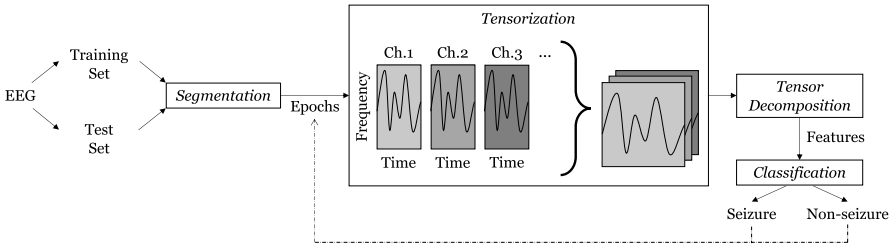

FIGURE 12.18

The block diagram of the proposed algorithm in [104] for seizure detection using tensor decomposition-based feature extraction.

In [106], EEG signals are recorded from multiple patients in 3-hour sessions that include the preictal period (before seizures take place) as well as the seizure. After applying fast Fourier transform, an STF tensor is obtained from each patient. The STF tensors are decomposed using CPD. In order to assess if any of the extracted components are related to the preictal period, a binary target vector showing the time instants of the preictal period is constructed. The correlation between the temporal signatures of all extracted components and the target is computed. Almost in all cases, a component that is significantly correlated to the preictal period is found. The spatial and spectral signatures of the preictal components suggest that a common structure might be involved in seizure generation, which can be useful in prediction of a seizure.

12.5.7 Connectivity analysis

Brain connectivity can be investigated in three subcategories, i.e., structural, functional, and effective connectivity (Fig. 12.19). Structural connectivity defines the existence of white matter tracts physically interconnecting brain regions whereas functional connectivity describes the statistical dependencies between neural signals acquired from different brain areas using measures such as correlation and coherence [107]. Effective connectivity can be considered as the combination of the two, as it attempts to extract networks quantifying the directional effects of one neural population on another one, characterized by axonal pathways [108].

12.5.7.1 Structural connectivity

In [109], a tensor network is proposed which shows the strength of white matter tracts between each pair of brain regions that are of interest. To start with, a tensor of size $M \times M \times S$ is constructed from DWI and MRI scans of S subjects covering M brain regions. For quantifying the relation between two regions, different features are tried, such as the fiber counts in-between or the water diffusivity along the fibers. Next, a semi-symmetric CPD is applied whose factors along the first two modes are equal ($\mathbf{u}_r^{(1)} = \mathbf{u}_r^{(2)}$) due to the symmetry of structural connectivity between two regions.

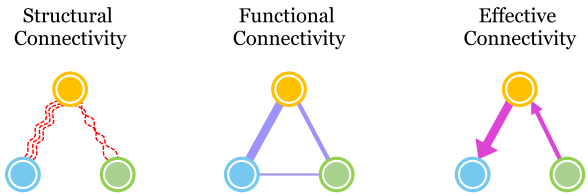

FIGURE 12.19

Types of brain connectivity [108]. Three brain regions are shown to be connected structurally (via fiber pathways), functionally (via statistical relations), and effectively (via information flow).

The number of components R is selected based on cumulative proportion of variation explained [110].

In order to discover a connectivity network that captures the most variation in the structural connectomes across all subjects, a weighted sum of $\mathbf{u}_r^{(1)}(\mathbf{u}_r^{(1)})^{\mathrm{T}}$ for $r = 1, 2, ..., R$ is calculated. Finally, the connectivity networks from different subject groups are compared. The obtained results reveal that stronger interconnections exist in the cortical area in people with positive traits, such as high language learning and motion ability, whereas weaker interactions exist in people with negative traits, such as use of alcohol.

12.5.7.2 Functional connectivity

Functional connectivity of the brain was assumed to be constant with respect to time until recently. As a consequence, functional connectivity networks (FCNs) were commonly represented with nodes that correspond to brain regions and edges that describe their pair-wise associations. After experimental studies that unveiled the time dependency of functional connectivity, dynamic FCNs have gained significant attention [111]. For dynamic FCNs where temporal information is incorporated as a third mode besides pairs of brain regions, tensors become the intrinsic representations.

In [112], the authors propose a tensor decomposition scheme for dynamic functional connectivity analysis on resting-state fMRI data. For this purpose, a tensor $\mathcal{X}$ of dimensions $M \times M \times W$ is constructed as shown in Fig. 12.20, where M is the number of brain regions and W is the number of time windows. The time windows are obtained by overlapping sliding windows over the time courses of investigated brain regions. For each time window w ($w = 1, 2, ..., W$), a matrix of size $M \times M$ showing the pair-wise connectivity values (computed using Pearson correlation or mutual information [113]) is constructed and placed into the w-th slice of $\mathcal{X}$.

Next, CPD is applied on $\mathcal{X}$, leading to factor matrices $\mathbf{U}^{(1)}$, $\mathbf{U}^{(2)}$, and $\mathbf{U}^{(3)}$ of dimensions $(M \times R)$, $(M \times R)$, and $(W \times R)$, respectively. Note that due to the assumed symmetry of functional connectivity between two regions, $\mathbf{U}^{(1)} = \mathbf{U}^{(2)}$. The columns of $\mathbf{U}^{(1)} = \mathbf{U}^{(2)}$ correspond to spatial signatures that are interpreted as connectivities. Both the input tensor and the approximated tensor obtained with CPD are denoised using binarization via thresholding.

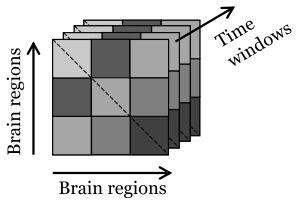

FIGURE 12.20

A 3D tensor model for dynamic functional connectivity [112]. The matrices at each slice showing pair-wise connectivity between brain regions are symmetric.

In order to find spatial maps that are common across subjects, K-means clustering is applied to the set of all spatial signatures extracted from all subjects. Finally, the cluster centers are assigned as prototype brain networks, which are found to be similar to several known resting state networks.

The model in Fig. 12.20 is extended with the *subject* mode in [114] for classification of multisubject fMRI data using MLSVD under two sets of conditions: (i) low vs. high walking speed in the elderly and (ii) resting vs. stress state in moderate-heavy alcohol consumers. The proposed approach is observed to provide a better classification accuracy than conventional SVD, which is applied after matricization of the original 4D tensor. MLSVD is also employed in [115] to analyze functional connectivity from fMRI data, but this time on a 3D tensor model with modes *connectivity*, *time*, and *subject*. In other words, unlike previous approaches, here the connectivity is not represented in a symmetric matrix form; instead, it is vectorized. The authors also propose a general linear model using the extracted temporal signatures to determine which connectivity maps are related to the experimental paradigm.

In [116], CPD is compared to Tucker decomposition for dynamic FCNs on resting-state multisubject fMRI data using sliding window correlation analysis. The authors conclude that although interpreting the components of CPD is more straightforward than interpreting those of Tucker decomposition, the Tucker model is often more effective for group differentiation.

Instead of using fixed-sized sliding windows, [117] proposes an approach to automatically determine different FCN states. The authors utilize a twofold algorithm to define the FCNs from a cognitive EEG study with multiple subjects. The first step is to identify the change points in time where the FCNs indicate a significant alteration. For this purpose, a low-rank approximation of the third-order tensor containing the pair-wise connectivities of a random subset of subjects at each time point is calculated via convex hull optimization [118], which selects an optimal value for the tensor rank. Tucker decomposition is applied to the tensors with the calculated rank value. Note that the factors along the first and second mode are equal ($\mathbf{U}^{(1)}(t) = \mathbf{U}^{(2)}(t)$) due to the symmetry of matrices at each slice. Finally, the subspace distance between consecutive (in time) basis elements of the decomposed matrices along the first mode is calculated as explained in [119]. The change points are detected by thresholding the distance (Fig. 12.21).

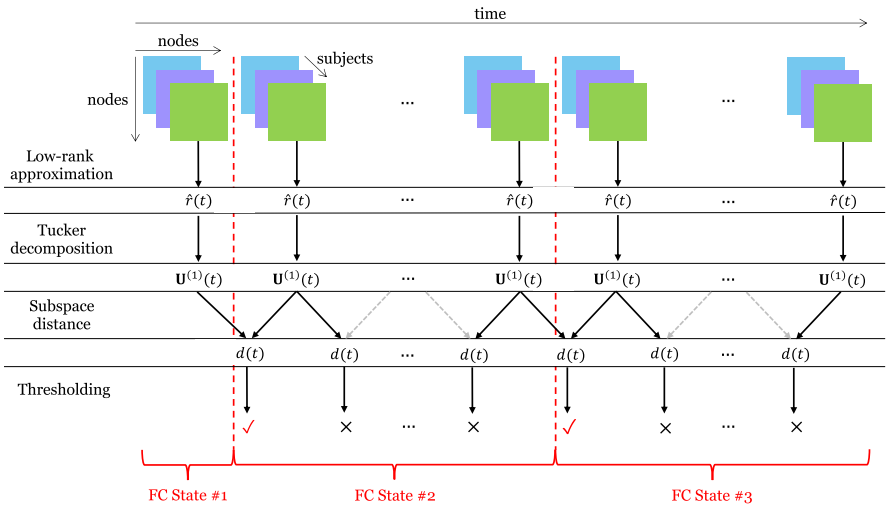

FIGURE 12.21

Steps of change detection in FCNs over an example [117]. Low-rank approximation is applied on the 3D tensors with a randomly selected subset of subjects at each time point to estimate their rank ($\hat{r}(t)$). Tucker decomposition is applied based on the rank values. The subspace distance $d(t)$ between the column subspaces obtained via Tucker decomposition ($\mathbf{U}^{(1)}(t)$) is calculated. Every distance value above a threshold yields a new functional connectivity state.

The change points define the time boundaries for functional connectivity states. The second task is to summarize the functional connectivity states inside these boundaries across subjects. Assuming that the functional connectivity states should remain stationary and common across subjects, the summarized states are obtained via tensor-matrix projections across time and space using another Tucker decomposition stage. The results demonstrate the formation of transient frontal networks during error processing.

In [120], PARAFAC2 is applied in the complex domain to compute functional connectivity by relating the extracted components to one another. For this purpose, received EEG signals are expressed as a linear mixture of multiple sources, which are modeled as auto-regressive (AR) processes. The EEG data are tensorized using short-time Fourier transform with Hanning windows, yielding three modes as *channel*, *complex frequency*, and *complex trial*. The connectivity metric is computed via a phase-lag index which estimates phase differences between trials that are extracted using PARAFAC2. PARAFAC2 adds the flexibility of expressing the trials in terms of frequency, and thus producing different connectivity maps for different frequency bands. On the other hand, [121] uses PARAFAC2 to obtain subject-specific network scaling as follows. First, functional connectivity is formulated as the covariance matrix of an fMRI data matrix (*voxels* $\times$ *time*). However, in order to obtain networks that are generalizable (among subjects) and interpretable, the data matrices

from each subject are first stacked into a 3D tensor and later decomposed into their low-rank components prior to covariance estimation. Using PARAFAC2, the strength of underlying networks is allowed to vary based on the subject.

Functional connectivity is an important field of research as changes in connectivity may serve as a biomarker in neurological disorders. This has been shown, for example, in [129] for autism spectrum disorder (ASD). The authors work on a third-order tensor of fractional amplitude of low-frequency fluctuations (fALFF) calculated for each voxel in an fMRI dataset. The metric fALFF characterizes the intensity of spontaneous brain activities and provides a measure of functional architecture of the brain. A linear tensor regression model is proposed by the authors, about which a more detailed explanation will follow in Section 12.5.8. Simply put, the image tensor serves as the observation whereas the subject's diagnosis status (as 0 [healthy] or 1 [having ASD]) and other variables such as age and sex form the covariate vector. The estimated coefficient tensors from healthy subjects and subjects who have ASD show clear distinctions in regions that are consistent with the autism literature such as the cerebellum, which is responsible for motor learning, coordination, cognitive functions, and effective regulation.

12.5.7.3 Effective connectivity

Functional connectivity explores the statistical similarities between the nodes in a physiological network, whereas effective connectivity searches for the direct (causal) interactions between them. Consequently, while describing effective connectivity, it is quite common to use multivariate AR modeling which expresses the dependency of the value of a node at a given time to the past values of all the nodes employed in the network.

For instance, [122] uses time-variant partial directed coherence (tvPDC) based on the Fourier transform of time-variant multivariate AR models on EEG data. The general form of a time-variant multivariate AR process of order P and with M nodes is expressed as [123]

$$\mathbf{x}(t) = \sum_{q=1}^{P} \mathbf{A}^{(q)}(t)\mathbf{x}(t-q) + \mathbf{e}(t), \tag{12.25}$$

where $\mathbf{x}(t) \in \mathbb{R}^M$ is the data vector at time t, $\mathbf{A}^{(q)}(t) \in \mathbb{R}^{M\times M}$ contains the q-th-order AR coefficients at time t, $\mathbf{e}(t) \in \mathbb{R}^M$ is the innovation noise, and the order P determines the total number of time lags included in the model.

The Fourier transform of the time-variant AR coefficients is defined as

$$\mathbf{A}(t, f) = \mathbf{I} - \sum_{q=1}^{P} \mathbf{A}^{(q)}(t)e^{-2\pi \mathrm{i} f r}, \tag{12.26}$$

where $\mathbf{I}$ is the identity matrix.

The degree of causal influence from node j to node i at time t and frequency f can then be quantified by tvPDC as follows:

$$\text{tvPDC}_{i\leftarrow j}(t,f)=\frac{|\mathbf{A}_{ij}(t,f)|}{\sqrt{\sum_{m=1}^{M}|\mathbf{A}_{mj}(t,f)|^2}}\in[0,1],\, i\neq j. \tag{12.27}$$

Hence, the tvPDC analysis of a single subject results in a 3D tensor containing the modes *space* (expressed for each node pair), *time*, and *frequency*. In order to enhance the interpretability of tvPDC analysis while incorporating an extra mode for different *subjects*, [122] proposes to apply CPD after obtaining the 4D tvPDC tensor from EEG data. The results show that the relation between the stimulus onset and signatures in temporal mode becomes more prominent in multisubject decomposition than in single-subject decomposition, meaning that the addition of the *subject* mode can provide critical input. In general, applying CPD on the tvPDC tensor is observed to reduce the amount of results to be investigated to a smaller but more informative subset, and this reduction can be taken even further by displaying the computed networks only if their associated content satisfies certain constraints. These constraints can be temporal resemblance to the onsets of a stimulus or be linked to a spectral window of interest.

Effective connectivity of the brain is studied on fMRI signals using Granger causality (GC) in [124]. GC is used to investigate the direction and magnitude of information flow between two simultaneously recorded time series [125].

Let the fMRI data matrix $\mathbf{X}$ be of size $M\times T$, where M is the total number of voxels and T is the number of time samples. Based on the multivariate AR model given in Eq. (12.25), [124] expresses the BOLD signal $\mathbf{x}_t=\mathbf{X}_{:t}$ for P time lags, only $\mathbf{A}^{(q)}(t)$ is replaced by $\mathbf{A}^{(q)}$, i.e., AR coefficients are not time-varying (referred to as spatial multivariate AR model). Any nonzero coefficient $\mathbf{A}_{ij}^{(q)}$ refers to the time series j (Granger) influencing time series i after q lags.

GC can be written as a tensor regression by extending Eq. (12.25) to multiple time samples $t=P+1,...,T+P$:

$$\mathbf{X}_{t-q}=[\mathbf{x}_{P+1-q},...,\mathbf{x}_{T+P-q}]^{\mathrm{T}}. \tag{12.28}$$

Then, by stacking all time lags ($q=1,...,P$) together, the data tensor $\boldsymbol{\mathcal{X}}\in\mathbb{R}^{P\times M\times T}$ and the AR coefficient tensor (i.e., the connectivity tensor) $\boldsymbol{\mathcal{A}}\in\mathbb{R}^{M\times M\times P}$ is obtained. Finally, the tensor regression based on the multivariate AR model is expressed as

$$\mathbf{X}_t=\boldsymbol{\mathcal{A}}\bullet_{\{M,P\}}\boldsymbol{\mathcal{X}}+\mathbf{E}_t, \tag{12.29}$$

where $\bullet_{M,P}$ shows tensor contraction over common dimensions M and P and $\mathbf{E}_t$ is the innovation noise. The connectivity tensor can be estimated as

$$\hat{\boldsymbol{\mathcal{A}}}=\arg\min_{\boldsymbol{\mathcal{A}}}\left\{||\mathbf{X}_t-\boldsymbol{\mathcal{A}}\bullet_{\{M,P\}}\boldsymbol{\mathcal{X}}||_2^2+\pi(\boldsymbol{\mathcal{A}})\right\}, \tag{12.30}$$

where $\pi(.)$ shows the penalty function.

Effective connectivity suggests structured sparsity on the connectivity tensor to avoid any forced connections. Therefore the authors posit a CPD structure for the connectivity tensor. The factors along the first, second, and third modes correspond to the spatial signature for receiving nodes, the spatial signature for sender nodes, and the temporal signature for causal lags, respectively.

12.5.8 Regression

Regression analysis aims to estimate the relationship between a set of dependent variables (i.e., the observations, responses, or outcomes) and independent variables (i.e., covariates, predictors, or explanatory variables). Particularly, the generalized linear model (GLM), which is a generalization of ordinary linear regression through a link function, is used for modeling in many areas of neuroimaging due to its flexible framework.

GLM is used to explain the expected value μ of the observation vector $\mathbf{y}$ given the matrix of covariates $\mathbf{X}$ with the help of regression coefficients ($\boldsymbol{\beta}$) and a link function $g(.)$ as follows [126]:

$$g(\mu) = g(\mathrm{E}(\mathbf{y}|\mathbf{X})) = \mathbf{X}\boldsymbol{\beta}. \tag{12.31}$$

Note that the ordinary linear regression model can be obtained by exploiting an identity link function. As observed from Eq. (12.31), classical regression methods treat each covariate as a vector (which are later concatenated in the matrix $\mathbf{X}$) while estimating the corresponding regression coefficients. However, new advances in neuroimaging require covariates of higher dimensions.

To adapt the GLM framework for higher-order data models, [127] proposes a generalized linear tensor regression model for a scalar observation y, a conventional covariate vector $\mathbf{z} \in \mathbb{R}^{I_0}$, and a general covariate tensor $\boldsymbol{\mathcal{X}} \in \mathbb{R}^{I_1 \times I_2 \times \ldots \times I_N}$:

$$g(\mu) = \alpha + \boldsymbol{\gamma}^{\mathrm{T}}\mathbf{z} + < \boldsymbol{\mathcal{B}}, \boldsymbol{\mathcal{X}} >, \tag{12.32}$$

where α is the intercept value, $\boldsymbol{\gamma} \in \mathbb{R}^{I_0}$ is the conventional regression coefficient vector, and $\boldsymbol{\mathcal{B}} \in \mathbb{R}^{I_1 \times I_2 \times \ldots \times I_N}$ is the coefficient tensor that captures the strength of the entries of the covariate tensor. In this model, clinical outcome (a binary value indicating the diagnosis status) is treated as the observation, multidimensional neuroimaging data (from 3D MR or 4D fMR images) correspond to the covariate tensor, and other predictors such as age and gender are included in the conventional covariate vector.

The challenge that comes with regressing such a model is its ultrahigh dimensionality. Therefore, the authors assume a low-rank structure of $\boldsymbol{\mathcal{B}}$ by expressing it with a rank-R CPD. This significantly reduces the dimensionality from $(I_0 + \prod_{n=1}^{N} I_n)$ to $(I_0 + R \times \sum_{n=1}^{N} I_n)$. Maximum likelihood estimation is performed for parameter prediction by introducing sparsity regularization that is used to identify subregions that are associated with the response traits.

This approach is adopted in [128] by representing the coefficient tensor $\boldsymbol{\mathcal{B}}$ with Tucker decomposition which provides a more flexible and practical model especially

in brain images with skewed dimensions as it allows a different number of factors along each mode, unlike CPD. The authors test their method on an attention deficit hyperactivity disorder dataset with T1-weighted MR images by first estimating the coefficient tensor from the training subjects and then predicting the clinical outcome for the rest of the subjects. Their results show that Tucker decomposition outperforms CPD in terms of classification accuracy.

Alternatively, [129] proposes to treat the observation as a tensor variable ($\mathcal{Y} \in \mathbb{R}^{I_1 \times I_2 \times \ldots \times I_N}$) instead of a scalar and expresses the linear tensor regression model as follows:

$$\mathcal{Y} = \mathcal{B} \times_{N+1} \mathbf{x} + \mathcal{E}, \tag{12.33}$$

where $\mathbf{x} \in \mathbb{R}^d$ is the covariate vector, $\mathcal{B} \in \mathbb{R}^{I_1 \times I_2 \times \ldots \times I_N \times d}$ is the $(N+1)$-th-order coefficient tensor, and $\mathcal{E} \in \mathbb{R}^{I_1 \times I_2 \times \ldots \times I_N}$ is the independent error tensor. Here, the brain image serves as the observation tensor, and the diagnosis status, age, gender, etc., form the covariate vector. The proposed method embeds two key sparse structures on $\mathcal{B}$, element-wise sparsity and low-rankness, through a weighted CPD. The prediction of weights and regression coefficients constitutes a nonconvex optimization problem, for which an alternating updating algorithm is developed. The authors use the proposed model on fMRI data to demonstrate the differences in functional brain connectivity caused by ASD (Section 12.5.7.2).

For regression of tensor observations on tensor predictors, a tensor subspace regression model, called higher-order partial least-squares (HOPLS), is proposed in [130]. To achieve this goal, a tensor subspace for both covariates and observations is constructed via Tucker decomposition. The authors test their method on simultaneously recorded EEG (scalp EEG, measured noninvasively) and ECoG (intracranial EEG, measured invasively) data, which are both represented as 4D arrays with modes *trial*, *channel*, *frequency*, and *time*. Their results show that HOPLS performs superior over ordinary PLS approaches for decoding of the ECoG data using EEG signals.

12.5.9 Feature extraction and classification

Feature extraction aims at summarizing the initial raw data using a smaller amount of entries which still capture their essence such that meaningful models can be learned from them in a more computationally efficient manner. From this perspective, it is not surprising that tensor decompositions, which can well approximate low-rank data using fewer parameters, are well suited for this task. Extracted features can later be used for classification purposes. Some topics related to feature extraction and classification (e.g., segmentation and seizure detection) or classification (e.g., binary regression algorithms) have been described in Section 12.5.3, Section 12.5.6.2, and Section 12.5.8; therefore, they will not be elaborated here. For details about the related works, aforementioned sections should be (re)visited.

CPD and Tucker decomposition are used to extract features for EEG-based classification of patients with Alzheimer's disease in [131]. To achieve this, an EEG tensor is constructed with modes *space*, *frequency*, and *subject* for both training and test

sets. First, *subject*-mode unfolding of the training tensor $\boldsymbol{\mathcal{X}}$ is approximated via a tensor decomposition. Using the factor matrices extracted from the rank-R CPD of $\boldsymbol{\mathcal{X}}$, mode-n unfolding matrix of $\boldsymbol{\mathcal{X}}$ can be expressed as

$$\mathbf{X}_{(n)} \approx \mathbf{U}^{(n)}[\mathbf{U}^{(N)} \odot \ldots \odot \mathbf{U}^{(n+1)} \odot \mathbf{U}^{(n-1)} \odot \ldots \odot \mathbf{U}^{(1)}]^{\mathrm{T}}, \tag{12.34}$$

$$\mathbf{X}_{(n)} \approx \mathbf{U}^{(n)}\mathbf{E}, \tag{12.35}$$

where $\odot$ shows the Khatri–Rao product. Here, $\mathbf{U}^{(n)}$ is a matrix of size $I_n \times R$ and holds R signatures of the unfolded mode n, each of which can be regarded as a feature vector. Therefore, $\mathbf{U}^{(n)}$ can be denoted as a feature matrix $\mathbf{F}$. For the given case $\mathbf{X}_{(\text{subject})}$ is computed, thus $\mathbf{F}$ holds the subject features. On the other hand, the encoding matrix $\mathbf{E}$ holds the information from *space* and *frequency* modes. The equivalent of encoding matrix in Tucker decomposition is given as the product of the core tensor with the factor matrices along *space* and *frequency*.

When unseen test data are received, a *subject*-mode unfolding matrix of the new tensor $\boldsymbol{\mathcal{Y}}$ is calculated by directly unfolding the tensor, denoted as $\mathbf{Y}_{(\text{subject})}$. The least-squares projection of the encoding matrix $\mathbf{E}$ on any $\mathbf{Y}_{(\text{subject})}$ returns the feature matrix $\mathbf{F}'$ of $\boldsymbol{\mathcal{Y}}$:

$$\mathbf{F}' = \mathbf{Y}_{(\text{subject})}\mathbf{E}^{\dagger}. \tag{12.36}$$

Finally, a feed-forward multilayer perceptron is used for classifying the feature matrices. Note that the proposed method reduces overall complexity by applying tensor decomposition to only the training data from which a dictionary is obtained and used for projecting on any unseen test data. The steps of this method are illustrated in Fig. 12.22.

A similar approach is utilized for drowsiness detection with EEG using a support vector machine classifier [132]. Furthermore, the authors propose a nonparametric Bayesian model to automatically determine the underlying CP rank by involving prior gamma distributions of factor matrices.

In [133], PARAFAC2 and CPD are used to extract refined composite multiscale entropy features from MEG data which are shown to differ between patients with Alzheimer's disease and healthy subjects. Another CPD-based feature extraction describing the mismatch negativity in EEG ERPs is defined in [134] to classify children with reading disability and attention deficit.

A multivariate TBM method is proposed in [135] for group-based classification of patients with Williams syndrome based on 3D MR images. First, individual surface deformation tensors are obtained by registering brain images to a common template. Since the resulting 3D maps provide many more features than the number of subjects included, a feature reduction step is found to be necessary. Consequently, a linear classifier is utilized to learn the feature weights with l_1-norm regularization which enforces sparsity on the surface features.

Another promising use of neural signal classification (besides for diagnostic purposes) is BCIs. A BCI receives brain signals from a subject and translates these signals to an external device that will take the subject's commands into action

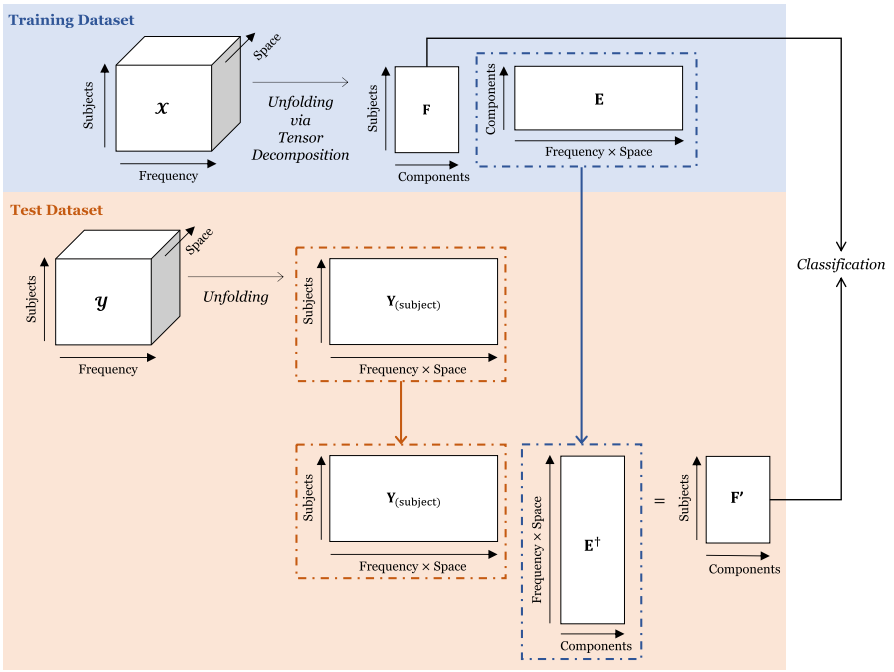

FIGURE 12.22

Feature extraction using an encoding matrix [131]. The encoding matrix $\mathbf{E}$ is calculated from the training dataset using CPD or Tucker decomposition (top row). The least-squares projection of the encoding matrix on the *subject*-mode unfolding matrix of any test dataset returns the new feature matrix $\mathbf{F}'$.

(Fig. 12.23). For instance, if a subject imagines to move his left arm, even if he does not actually move it, his neural activation will still point out that he wishes to do so. This way, by establishing a connection with the recording device, a robot arm can realize the desired movement for the subject. BCIs can be driven by mental imagination of an activity (such as motor imagery) or by responses to external stimuli (such as P300 and steady-state visually evoked potentials [SSVEPs]).

The main paradigms used by the vast majority of BCIs are motor imagery, P300, and SSVEP. In motor imagery, subjects imagine themselves moving their body parts, which creates event-related (de)synchronizations in sensorimotor areas. P300-based BCI takes its name from the P300 wave, which is a type of ERP that occurs in the human brain as a positive deflection with a time delay of around 300 ms after a specific auditory, visual, or somatosensory event has taken place. SSVEPs are evoked in the occipital cortex when the user concentrates on flickering visual stimuli [136].

For classifying left and right hand imagery movement, CPD and Tucker decomposition of 4D EEG tensors with modes *frequency* (based on Morlet wavelets), *time*, *channel*, and *trial* is proposed in [137]. Both techniques are reported to outperform

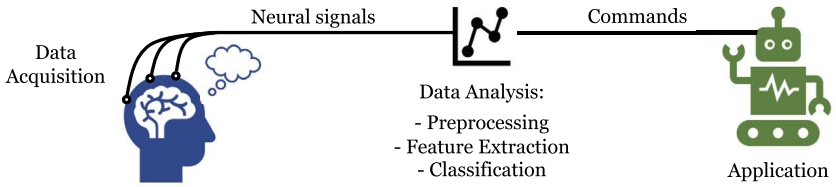

FIGURE 12.23

Illustration of BCIs. BCIs convert the subject's neural signals to commands that control external devices.

common spatial pattern (CSP) filtering. CSP filtering finds spatial filters that maximize the variance of the filtered signal for one class and minimize for the other using training set labels [138]. Alternatively, a 4D EEG tensor consisting of modes *frequency* (based on Morlet wavelets), *time*, *channel*, and *condition* is decomposed using CPD and Tucker decomposition in [139] for the same imagery movement problem. To extract the most discriminative components for different classes (left hand or right hand), sparseness is imposed on the condition mode. The resulting components unveil differences across conditions in channel, time, and frequency signatures; for example, the components that correspond to imagined motor tasks covering sensorimotor areas reveal symmetrical behavior in their topography and condition modes as expected, i.e., the left class shows a higher amplitude (than the right class) when the left hemisphere is active, and vice versa. The authors however note that the proposed offline method should be extended for dynamic and window-based time analysis in order to capture the changing neural streams over time.

An online BCI system for predicting left and right hand imagery movement is combined with several tensor completion algorithms (Section 12.5.1) to analyze a rather flawed EEG dataset along modes *time*, *channel*, and *trial* that includes corrupted entries and channels in [43]. Feature vectors are extracted from the completed tensors using CSP filtering. To evaluate the improvement achieved by each algorithm, linear discriminant analysis and linear support vector machine classification is utilized. For each subject, the first run is recorded where a cue (left or right arrow) is shown to the subject and used to train the classifier. The system also gives an online feedback by showing the result of classification.

Single-trial EEG classification remains a challenging but important task in BCI applications, considering that it offers a more convenient and faster framework for the subjects. Taking into the account the low number of training samples and high dimensionality of the data in such a case, [140] proposes spectral regularization using the nuclear norm due to the fact that it conveys a priori structural information. To construct the tensorial EEG model, first each channel is segmented into time windows. For each channel, the Hankel matrix of a feature vector containing mean signal amplitudes of each time window is calculated. Channel Hankel matrices are stacked to obtain the EEG tensor. Compared to linear discriminant analysis with shrinkage applied to the feature vector, nuclear norm regularization on tensorial EEG is ob-

served to perform significantly better in classifying P300 ERPs in an auditory oddball paradigm.

In [141], multilinear discriminant analysis of an EEG feature tensor is proposed to classify ERPs from a visual P300-based BCI experiment, in which a matrix of letters is presented to the subjects who silently count how many times the indicated target letter is intensified. The feature tensor is constructed by appending degrees of polynomial fittings for each channel and time segment.

In order to carry BCIs to a practical real-life use, there are two main challenges: subject mobility and subject-specific calibrations (such as in [43] mentioned above). A subject-specific calibration-free method for mobile BCI is proposed based on CPD and BTD of EEG data in [142] with P300 auditory oddball paradigm. For this purpose, the average ERP of all subjects except one is calculated during baseline and target stimuli. This way, two template matrices (one for the baseline and one for target stimuli) are constructed with modes *channel* and *time*. Each trial pair (with the same modes as the templates) of the unknown subject are stacked into a tensor and appended with the baseline and target template obtained from all other subjects to construct the final 3D tensor. The addition of these templates to the trial pair data tensor enhances the likelihood of extracting a task-related signature. After decomposition, the value in the trial-mode signature cues the presence of the target. The classification results are observed to be similar to subject-specific trained models.

Another subject-specific calibration-free classification for an SSVEP-based BCI experiment is proposed in [143] using CPD on a 4D EEG tensor with modes *trial*, *space*, *frequency*, and *subject*. The experiment involves a left and right button flashing with different frequencies and the objective is to identify which button the subject is focused on at a given time. Nonnegativity is enforced in the *trial*, *space*, and *subject* modes which facilitates their interpretation while orthogonality is imposed on the *frequency* mode which guarantees linear independence between factors representing the distinct frequency SSVEP peaks. The rank of CPD is kept constant at 3 so that distinct factors for the two SSVEP signals of interest could be uniquely described whereas the third factor can account for background activity. The factor matrices obtained by decomposing the training tensor along the *space* and *frequency* modes ($\mathbf{U}^{(2)}$ and $\mathbf{U}^{(3)}$, respectively) are used to define the encoding matrix $\mathbf{E} = [\mathbf{U}^{(2)} \odot \mathbf{U}^{(3)}]^{\mathrm{T}}$, which is projected on data tensors from new subjects and trials as described above ([131]).

A method based on l_1-regularized multiway canonical correlation analysis (multiway CCA [MCCA]) for an SSVEP-based BCI with frequencies $f_1, ..., f_M$ is proposed in [144]. CCA attempts to find a pair of linear transforms for two random variables that maximize the correlation coefficient between them. In the training stage, 3D EEG tensors $\boldsymbol{\mathcal{X}}^{(m)}$ (*channel* $\times$ *time* $\times$ *trial*) whose trials belong to a specific frequency f_m and matrices $\mathbf{Y}^{(m)}$ (*harmonic* $\times$ *time*) which store the harmonics of f_m are constructed. The l_1-regularized MCCA searches for the optimum linear transforms in *channel* and *trial* modes for $\boldsymbol{\mathcal{X}}^{(m)}$ and in *harmonic* mode for $\mathbf{Y}^{(m)}$ as

follows:

$$\mathbf{w}_1^{(m)}, \mathbf{w}_3^{(m)}, \mathbf{v}^{(m)} = \underset{\mathbf{w}_1, \mathbf{w}_3, \mathbf{v}}{\arg\min} \frac{1}{2} ||\boldsymbol{\mathcal{X}}^{(m)} \times_1 \mathbf{w}_1^{\mathrm{T}} \times_3 \mathbf{w}_3^{\mathrm{T}} - \mathbf{v}^{\mathrm{T}} \mathbf{Y}^{(m)}||_2^2 \tag{12.37}$$

$$+ \lambda_1 ||\mathbf{w}_1||_1 + \lambda_2 ||\mathbf{v}||_1 + \lambda_3 ||\mathbf{w}_3||_1 \tag{12.38}$$

$$\text{s.t. } ||\mathbf{w}_1||_2 = ||\mathbf{v}||_2 = ||\mathbf{w}_3||_2 = 1, \tag{12.39}$$

where λ_1, λ_2, and λ_3 are regularization parameters to control the sparsity of the linear transforms $\mathbf{w}_1$, $\mathbf{v}$, and $\mathbf{w}_3$ respectively. The results produce one optimized reference vector for each frequency as $\mathbf{z}^{(m)} = \boldsymbol{\mathcal{X}}^{(m)} \times_1 (\mathbf{w}_1^{(m)})^{\mathrm{T}} \times_3 (\mathbf{w}_3^{(m)})^{\mathrm{T}}$. When a single-trial data ($\mathbf{X}$: *channel* $\times$ *time*) is received, the CCA coefficient ρ_m between $\mathbf{X}$ and $\mathbf{z}^{(m)}$, $m = 1, ..., M$, is calculated. Finally, the frequency of the trial is estimated by $\hat{m} = \arg\max_m \rho_m$, and thus $\hat{f} = f_{\hat{m}}$. The block diagram of the proposed method is demonstrated in Fig. 12.24.

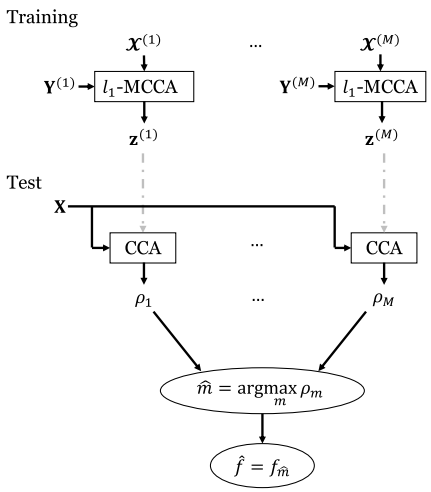

FIGURE 12.24

Steps of l_1-MCCA for SSVEP-based BCI [144]. During training, optimal reference signals $\mathbf{z}^{(m)}$ are learned by applying l_1-MCCA between $\boldsymbol{\mathcal{X}}^{(m)}$ (from multiple trials) and $\mathbf{Y}^{(m)}$ for each frequency index m. For new single-trial data $\mathbf{X}$, the CCA between $\mathbf{X}$ and each $\mathbf{z}^{(m)}$ is calculated. The frequency of the new SSVEP trial is estimated as the one leading to the highest CCA coefficient.

12.5.10 Summary and practical considerations

The multiway structure of the brain, including various modes that are introduced by the experimental designs (such as multiple subjects, conditions, trials, etc.) or by the imaging modality (such as the use of different wavelengths in fNIRS) or incorporated during analysis for a more comprehensive capture of the underlying dynamics

(such as frequency expansion via wavelet transform), designates the use of tensors as the intuitive approach for modeling and processing of neuroimaging data. Moreover, comparative studies that evaluate the performance of tensors with respect to their 1D or 2D alternatives show that tensors reveal better results in numerous applications ranging from dimensionality reduction [57] and seizure localization [99] to segmentation [59] and analysis of brain connectivity [114]. Tensor-based solutions for neuroimaging applications reviewed in this chapter are listed in Table 12.1 according to the imaging modality.

In terms of practicality of tensor decompositions, there exist several challenges that can be categorized under the correct choice of rank, components of interest, and initial parameters.

Various approaches have been utilized so far for automatic determination of rank. These include the core consistency diagnostic [90], cumulative proportion of variation explained [109], minimization of the dimensionality of the latent space as described in a Bayesian framework [39], and truncation based on the MLSVD core [104] or based on eigenvalues of the measurement covariances [59].

In addition, some applications require selecting a subset of extracted components, such as for removal of artifact terms, dimensionality reduction, seizure localization, or connectivity analysis. For instance, [90] orders components according to their variance to automatically determine the dominant (epileptic) component, whereas [47] defines an a priori frequency band separating the noise and signal subspaces for automatic removal of residual water in MRS images. Alternatively, [122] proposes to extract only the FCNs that are related to the experimental paradigm, i.e., whose temporal signatures follow the stimulus onsets. Even when component selections are made based on external clinical input, significant differences are observed between signatures belonging to different activity components [100]. The more field expertise or previous empirical findings about the activities of interest are embraced as prior knowledge, the more informed and stable decisions can be made while automating component selection.

Last but not least, as with any optimization problem, good initialization is required to ensure convergence to global optima. Optimization-based tensor decomposition algorithms require any factor matrices and core tensors involved to be initialized. Tensorlab [145] offers internally integrated initialization method(s) for CPD, MLSVD, and $(L_r, L_r, 1)$-BTD based on randomized SVD with randomized subspace iterations to approximate the SVDs of tensor unfoldings. The same method can be used in structured data fusion to reduce the computation time. Another general option is to initialize all values randomly (most likely multiple times, among which the best-cost solution should be determined). For example, [47] uses a quality metric to evaluate the decomposition result based on the variance of component subspaces, which, if found poorly, sends a feedback for reinitialization. Alternatively, the results from a previous decomposition run can be used to initialize a new run [124].

In summary, tensors can be very powerful tools for analyzing multidimensional neuroimaging data, but their success depends on well-informed and appropriate choices for the critical steps explained above.

Table 12.1 A summary of the tensor-based algorithms reviewed in this work with their corresponding applications to neuroimaging data.

Neuroimaging modality	Tensor-based analysis	Application
EEG	CPD, PARAFAC2	Filling in missing data [38,40,43], denoising, artifact removal, and dimensionality reduction [57], source separation [77,82], activity recognition and source localization [87–93,100,101,104,106], connectivity analysis [120,122], feature extraction and classification [43,131,132,134,137,139,142,143]
	Tucker, MLSVD	Denoising, artifact removal, and dimensionality reduction [100], activity recognition and source localization [99,104], connectivity analysis [117], regression [130], feature extraction and classification [131,137,139]
	BTD	Activity recognition and source localization [103,104], feature extraction and classification [142]
	MCCA	Feature extraction and classification [144]
MRI (and variants)	TBM	Registration and longitudinal analysis [70–74], feature extraction and classification [135]
	CPD	Filling in missing data [41], denoising, artifact removal, and dimensionality reduction [40,54], segmentation [59,60,63,66], registration and longitudinal analysis [75], connectivity analysis [109], regression [127]
	Tucker, MLSVD	Denoising, artifact removal, and dimensionality reduction [47,58,63], segmentation [62,63], regression [128]
fMRI	CPD, PARAFAC2	Source separation [78], connectivity analysis [112,116,121,124,129], regression [127,129]
	Tucker, MLSVD	Connectivity analysis [114–116]
	BTD, BTD2	Source separation [78]
fNIRS	CPD	Denoising, artifact removal, and dimensionality reduction [52,53], activity recognition and source localization [52,94]
PET	Tensor SVD	Denoising, artifact removal, and dimensionality reduction [55]
fUS	BTD	Source separation [81]
MEG	CPD, PARAFAC2	Feature extraction and classification [133]

12.6 Future challenges

Evolution of medical technology, as well as the ever-increasing demand for it, has led to escalating data sizes with higher spatiotemporal resolution, longer recordings, and a rising number of patients. By 2020, the amount of health care data worldwide has reached 25,000 petabytes, whereas it amounted to approximately 500 petabytes in 2012 [146]. The availability of data at such a large quantity encourages the development of data-driven approaches for medical care purposes. These include patient diagnoses, treatments, and continuous monitoring of patients' health status. Inevitably, the future of medical care relies on Big Data solutions.

Indeed, during the last decade we witnessed the power and effectiveness of deep learning methods in solving very complex tasks using vast amounts of available training data [147]. This is true in particular for image processing, including medical imaging. However, deep learning falls short in transparency: its decision structure is highly complex and nonlinear, and therefore not interpretable. Understanding how and why a certain decision is made, however, is crucial in medical decision support systems in order to maintain trust and avoid unexpected behavior [148]. We believe that tensors can play a role in making deep learning solutions more transparent. Indeed, a series of theoretical research studies has shown links between (deep) neural networks and tensor decompositions. Their results suggest that, by analyzing and modeling certain classes of deep neural networks (DNNs) using tensor tools, we obtain simpler network structures of enhanced expressive power and reduced complexity [149].

Reduced complexity is not only important for transparency; it is also crucial for computational efficiency. When the input data are high-dimensional, the number of entries and hence the number of DNN parameters become intractable. This problem is referred to as the curse of dimensionality: the number of entries in a tensor grows exponentially with its order. Dimensionality reduction using MLSVD (as described in Section 12.5.2) may not be helpful: the core tensor, having the same order as the original tensor, still has a large number of entries even in the case of low multilinear rank [150]. Tensor trains overcome this problem by expressing a high-order tensor as a series of tensor contractions between consecutive low (typically second and third)-order tensors [151]. Tensor trains are still scarcely used in biomedical signal processing. A remarkable application for whole-brain fMRI pattern recognition is presented in [152], where the weight matrix of the fully connected layer of a neural network is compressed via a tensor train.

In many applications it is easy to collect large amounts of normal and healthy data, but abnormal examples, such as rare diseases or epileptic seizures, are scarce. This results in unbalanced training data, which is a challenging machine learning problem. In order to be able to learn and generalize from a few examples in the target class, the machine learning model can benefit from prior knowledge based on expert input. In practice, the prior knowledge can be incorporated in the form of constraints in the optimization problem. The constraint reduces the solution search space and therefore helps to converge to the global minimum. As real-life data are often

low-rank, a simple regularization using the trace norm (i.e., the convex relaxation of the rank function) or its tensorial extensions can already be helpful [153,154]. When more specific knowledge is available (e.g., sparsity, nonnegativity, or a parametric generating function), these can be conveyed via explicit constraints such as sparsity, nonnegativity, or a parametric generating function [155]. As tensors can admit different constraints along each of their modes simultaneously [21], they are especially fit for this task.

Many studies that have been performed on multiple subjects highlight the necessity to deliver personalized health care and medicine, taking into consideration each patient's medical history and even their genetics [156]. In this context, multimodal fusion will gain importance. We believe that tensor techniques will play an important role here as well, as they allow to handle heterogeneous data (e.g., EEG, structural images, and phenotypic scores [157]) simultaneously and—again—to impose constraints that ensure interpretability.

Tensors were formulated in 1900 [158], but it was only in the last few decades that they have been extensively recognized by the signal processing and machine learning community. In our opinion, the use of tensor tools at their full potential, especially in applied and clinical contexts, depends on two crucial factors. Good software tools are needed and the users of such tools have to be appropriately educated about their use.

There are various software toolboxes available that allow novice users to apply standard tensor decomposition structures. For an overview, see [150]. These allow quick prototyping and testing of new tensor models, and some offer heuristics for practical choices. However, as the complexity of the model increases (e.g., coupled factorizations and constraints) the computational time needed to solve the optimization problems becomes excessive. Before such tensor tools can be used in practice, custom-made efficient optimization algorithms are needed. The practical challenges outlined in Section 12.5.10 also become more pronounced. Therefore, young researchers should be provided with in-depth training material about the correct use and interpretation of tensor models. Tensor overview articles such as [28], [150], and [159] contribute well to this objective. We believe that tensors will become an increasingly tackled topic in the near future at workshops, tutorials, and summer schools and as elective courses in electrical, computer, and mathematical engineering curricula.

12.7 Conclusion

This chapter provides a general overview on the use of tensors for a wide range of neuroimaging applications. When experimental data are inherently multidimensional, 1D or 2D methods that require unfolding of the original tensor are not fully capable of representing all variations and interplay of the data in each mode. Meanwhile, multidimensionality is an indispensable property of neural data, especially if one wishes to obtain results that are generalizable, such as over multiple subjects, trials, or

conditions. Furthermore, keeping the natural formation of the data makes individual structuring of its modes and interpretation of the modeling and results simpler.

Tensor-based solutions exist in all stages of the neural signal processing pipeline, ranging from denoising and dimensionality reduction to BCIs. As with any mathematical algorithm, one might face several challenges when using a tensor-based method, such as parameter selection. However, with a correct understanding of the nature of input neural data and, accordingly, an appropriate choice of the tensor tool, it has been possible to build completely data-driven end-to-end systems. In this chapter, we aimed to list existing employments of tensors in neuroimaging, along with several reasons why we expect to see more of tensors while addressing the needs of future medical technology regarding Big Data applications in diagnosis and monitoring of patients, providing them with the right personalized medical care.

References

[1] R. Marino Jr., M. Gonzales-Portillo, Preconquest Peruvian neurosurgeons: a study of inca and pre-Columbian trephination and the art of medicine in ancient Peru, Neurosurgery 47 (4) (2000) 940–950.

[2] O.I. Abiodun, A. Jantan, O.E. Omolara, K. Dada, N. Mohamed, H. Arshad, State-of-the-art in artificial neural network applications: a survey, Heliyon 4 (11) (2018) e00938.

[3] G.V. Hirsch, C.M. Bauer, L.B. Merabet, Using structural and functional brain imaging to uncover how the brain adapts to blindness, Annals of Neuroscience and Psychology 2 (5) (2015).

[4] S.A. Bunge, I. Kahn, Cognition: An overview of neuroimaging techniques, Encyclopedia of Neuroscience (2009) 1063–1067.

[5] A.M. Aisen, W. Martel, E.M. Braunstein, K.I. McMillin, W.A. Phillips, T.F. Kling, MRI and CT evaluation of primary bone and soft-tissue tumors, American Journal of Roentgenology 146 (4) (1986) 749–756.

[6] J.M. Soares, P. Marques, V. Alves, N. Sousa, A Hitchhiker's guide to diffusion tensor imaging, Frontiers in Neuroscience 7 (2013) 31.

[7] T. Neumann-Haefelin, H.J. Wittsack, F. Wenserski, M. Siebler, R.J. Seitz, U. Mödder, H.J. Freund, Diffusion- and perfusion-weighted MRI. The DWI/PWI mismatch region in acute stroke, Stroke 30 (8) (1999) 1591–1597.

[8] A.E. Pereda, Electrical synapses and their functional interactions with chemical synapses, Nature Reviews. Neuroscience 15 (2014) 260–263.

[9] H. Berger, Über das Elektrenkephalogramm des Menschen, Archiv für Psychiatrie und Nervenkrankheiten 87 (1929) 527–570.

[10] S.P. Sanjay, Magnetoencephalography: basic principles, Annals of Indian Academy of Neurology 17 (1) (2014) 107–112.

[11] C. Huneau, H. Benali, Hugues Chabriat, Investigating human neurovascular coupling using functional neuroimaging: a critical review of dynamic models, Frontiers in Neuroscience 9 (2015) 467.

[12] H.T. Chugani, M.E. Phelps, J.C. Mazziotta, Positron emission tomography study of human brain functional development, Annals of Neurology 22 (4) (1987) 487–497.

[13] J.B. Balardin, G.A. Zimeo Morais, R.A. Furucho, L. Trambaiolli, P. Vanzella, C. Biazoli Jr, J.R. Sato, Imaging brain function with functional near-infrared spectroscopy in unconstrained environments, Frontiers in Human Neuroscience 11 (2017) 258.

[14] G.H. Glover, Overview of functional magnetic resonance imaging, Neurosurgery Clinics of North America 22 (2) (2011) 133–139.

[15] E. Macé, G. Montaldo, I. Cohen, M. Baulac, M. Fink, M. Tanter, Functional ultrasound imaging of the brain, Nature Methods 8 (2011) 662–664.

[16] T. Deffieux, C. Demené, M. Pernot, M. Tanter, Functional ultrasound neuroimaging: a review of the preclinical and clinical state of the art, Current Opinion in Neurobiology 50 (2018) 128–135.

[17] G. Northoff, Z. Huang, How do the brain's time and space mediate consciousness and its different dimensions? Temporo-spatial theory of consciousness (TTC), Neuroscience & Biobehavioral Reviews 80 (2017) 630–645.

[18] E. Acar, Y. Levin-Schwartz, V.D. Calhoun, T. Adali, ACMTF for fusion of multi-modal neuroimaging data and identification of biomarkers, in: 2017 25th European Signal Processing Conference (EUSIPCO), 2017, pp. 643–647.

[19] F. Cong, Q. Lin, L. Kuang, X. Gong, P. Astikainen, T. Ristaniemi, Tensor decomposition of EEG signals: a brief review, Journal of Neuroscience Methods 248 (2015) 59–69.

[20] C.F. Beckmann, S.M. Smith, Tensorial extensions of independent component analysis for multisubject FMRI analysis, NeuroImage 25 (1) (2005) 294–311.

[21] L. Sorber, M. Van Barel, L. De Lathauwer, Structured data fusion, IEEE Journal of Selected Topics in Signal Processing 9 (4) (2015) 586–600.

[22] Y. Murin, J. Kim, J. Parvizi, A. Goldsmith, SozRank: A new approach for localizing the epileptic seizure onset zone, PLoS Computational Biology 14 (1) (2018) e1005953.

[23] W.S. Sohn, K. Yoo, Y.B. Lee, S.W. Seo, D.L. Na, Y. Jeong, Influence of ROI selection on resting state functional connectivity: an individualized approach for resting state fMRI analysis, Frontiers in Neuroscience 9 (2018) 280.

[24] D. Gajic, Z. Djurovic, J. Gligorijevic, S. Di Gennaro, I.M.S. Gajic, Detection of epileptiform activity in EEG signals based on time-frequency and non-linear analysis, Frontiers in Computational Neuroscience 9 (2015) 38.

[25] C. Chatzichristos, K. Eleftherios, Y. Kopsinis, M. Morante, S. Theodoridis, Higher-order block term decomposition for spatially folded fMRI data, Lecture Notes in Computer Science (2017) 3–15.

[26] D. Kalman, A singularly valuable decomposition: the SVD of a matrix, The College Mathematics Journal 27 (1) (1996) 2–23.

[27] A. Zhang, D. Xia, Tensor SVD: statistical and computational limits, IEEE Transactions on Information Theory 64 (11) (2018) 7311–7338.

[28] T.G. Kolda, B.W. Wader, Tensor decompositions and applications, SIAM Review 51 (3) (2009) 455–500.

[29] J.H.de M. Goulart, M. Boizard, R. Boyer, G. Favier, P. Comon, Tensor CP decomposition with structured factor matrices: algorithms and performance, IEEE Journal of Selected Topics in Signal Processing 10 (4) (2016) 757–769.

[30] A. Cichocki, D.P. Mandic, A. Phan, C.F. Caiafa, G. Zhou, Q. Zhao, L. De Lathauwer, Tensor decompositions for signal processing applications from two-way to multiway component analysis, IEEE Signal Processing Magazine 32 (2) (2014) 145–163.

[31] H.A.L. Kiers, J.M.F. ten Berge, R. Bro, PARAFAC2—Part I. A direct fitting algorithm for the PARAFAC2 model, Journal of Chemometrics 13 (3) (1998) 275–294.

[32] I. Perros, E.E. Papalexakis, F. Wang, R. Vuduc, E. Searles, M. Thompson, J. Sun, SPARTan: Scalable PARAFAC2 for large & sparse data, in: Proceedings of the 23rd ACM SIGKDD International Conference on Knowledge Discovery and Data Mining, 2017, pp. 375–384.

[33] L. De Lathauwer, B. De Moor, J. Vandewalle, A multilinear singular value decomposition, SIAM Journal on Matrix Analysis and Applications 21 (4) (2000) 1253–1278.

[34] G. Bergqvist, E.G. Larsson, The higher-order singular value decomposition: theory and an application [lecture notes], IEEE Signal Processing Magazine 27 (3) (2010) 151–154.

[35] J. Chen, Y. Saad, On the tensor SVD and the optimal low rank orthogonal approximation of tensors, SIAM Journal on Matrix Analysis and Applications 30 (4) (2008) 1709–1734.

[36] N. Hao, M. Kilmer, K. Braman, R. Hoover, Facial recognition using tensor-tensor decompositions, SIAM Journal on Imaging Sciences 6 (1) (2013) 437–463.

[37] L. Sorber, M. Van Barel, L. De Lathauwer, Optimization-based algorithms for tensor decompositions: canonical polyadic decomposition, decomposition in rank-(lr, lr, 1) terms, and a new generalization, SIAM Journal on Optimization 23 (2) (2013) 695–720.

[38] E. Acar, D.M. Dunlavy, T.G. Kolda, M. Mørup, Scalable tensor factorizations with missing data, in: Proceedings of the SIAM International Conference on Data Mining, 2010, pp. 701–712.

[39] Q. Zhao, G. Zhou, L. Zhang, A. Cichocki, S. Amari, Bayesian robust tensor factorization for incomplete multiway data, IEEE Transactions on Neural Networks and Learning Systems 27 (4) (2010) 736–748.

[40] G. Cui, L. Zhu, L. Gui, Q. Zhao, J. Zhang, J. Cao, Multidimensional clinical data denoising via Bayesian CP factorization, Science China. Technological Sciences 63 (2019) 249–254.

[41] J.A. Bazerque, G. Mateos, G.B. Giannakis, Rank regularization and Bayesian inference for tensor completion and extrapolation, IEEE Transactions on Signal Processing 61 (22) (2013) 5689–5703.

[42] S. Friedland, L. Lim, Nuclear norm of higher-order tensors, Mathematics of Computation 87 (311) (2017) 1255–1281.

[43] J. Solé-Casals, C.F. Caiafa, Q. Zhao, A. Cichocki, Brain-computer interface with corrupted EEG data: a tensor completion approach, Cognitive Computation 10 (2018) 1062–1074.

[44] C. Caiafa, A. Cichocki, Multidimensional compressed sensing and their applications, Data Mining and Knowledge Discovery 3 (6) (2013) 355–380.

[45] J. Liu, P. Musialski, P. Wonka, J. Ye, Tensor completion for estimating missing values in visual data, IEEE Transactions on Pattern Analysis and Machine Intelligence 35 (1) (2013) 208–220.

[46] H. Zhu, R. Ouwerkerk, P.B. Barker, Dual-band water and lipid suppression for MR spectroscopic imaging at 3 tesla, Magnetic Resonance in Medicine 63 (6) (2010) 1486–1492.

[47] H.N. Bharath, O. Debals, D.M. Sima, U. Himmelreich, L. De Lathauwer, S. Van Huffel, Tensor-based method for residual water suppression in ^{1}h magnetic resonance spectroscopic imaging, IEEE Transactions on Biomedical Engineering 66 (2) (2019) 584–594.

[48] R.J. Croft, R.J. Barry, Removal of ocular artifact from the EEG: a review, Clinical Neurophysiology 30 (1) (2000) 5–19.

[49] S. Ge, M. Han, X. Hong, A fully automatic ocular artifact removal from EEG based on fourth-order tensor method, Biomedical Engineering Letters 4 (2014) 55–63.

[50] L. De Lathauwer, J. Castaing, J. Cardoso, Fourth-order cumulant-based blind identification of underdetermined mixtures, IEEE Transactions on Signal Processing 55 (6) (2007) 2965–2973.
[51] R.J. Cooper, J. Selb, L. Gagnon, D. Phillip, H.W. Schytz, H.K. Iversen, M. Ashina, D.A. Boas, A systematic comparison of motion artifact correction techniques for functional near-infrared spectroscopy, Frontiers in Neuroscience 6 (2012) 147.
[52] A. Hüsser, L. Caron-Desrochers, J. Tremblay, P. Vannasing, E. Martínez-Montes, A. Gallagher, Parallel Factor Analysis (PARAFAC) for Multidimensional Decomposition of FNIRS Data – a Validation Study, bioRxiv, 806778, 2019.
[53] J. Tremblay, E. Martínez-Montes, A. Hüsser, L. Caron-Desrochers, P. Pouliot, P. Vannasing, A. Gallagher, LIONirs: Flexible Matlab Toolbox for fNIRS Data Analysis, bioRxiv, 2020.09.11.257634, 2020.
[54] L. Ying, Y.M. Zou, D.P. Klemer, J. Wang, Determination of fiber orientation in MRI diffusion tensor imaging based on higher-order tensor decomposition, in: 2007 29th Annual International Conference of the IEEE Engineering in Medicine and Biology Society, 2007, pp. 2065–2068.
[55] N. Xie, Y. Chen, H. Liu, 3D tensor based nonlocal low rank approximation in dynamic PET reconstruction, Sensors 19 (23) (2019) 1–20.
[56] C. Lu, J. Feng, W. Liu, Z. Lin, S. Yan, Tensor robust principal component analysis with a new tensor nuclear norm, IEEE Transactions on Pattern Analysis and Machine Intelligence 42 (4) (2020) 925–938.
[57] M. Taherisadr, M. Joneidi, N. Rahnavard, EEG signal dimensionality reduction and classification using tensor decomposition and deep convolutional neural networks, in: 2019 IEEE 29th International Workshop on Machine Learning for Signal Processing (MLSP), 2019, pp. 1–6.
[58] Y. Yu, J. Jin, F. Liu, S. Crozier, Multidimensional compressed sensing MRI using tensor decomposition-based sparsifying transform, PLoS ONE 9 (6) (2014) e98441.
[59] H.N. Bharath, D.M. Sima, N. Sauwen, U. Himmelreich, L. De Lathauwer, S. Van Huffel, Nonnegative canonical polyadic decomposition for tissue-type differentiation in gliomas, IEEE Journal of Biomedical and Health Informatics 21 (4) (2017) 1124–1132.
[60] H.N. Bharath, N. Sauwen, D.M. Sima, U. Himmelreich, L. De Lathauwer, S. Van Huffel, Canonical polyadic decomposition for tissue type differentiation using multi-parametric MRI in high-grade gliomas, in: 2016 24th European Signal Processing Conference (EUSIPCO), 2017, pp. 547–551.
[61] M. Sørensen, L. De Lathauwer, Blind signal separation via tensor decomposition with Vandermonde factor: canonical polyadic decomposition, IEEE Transactions on Signal Processing 61 (22) (2013) 5507–5519.
[62] H.N. Bharath, S. Colleman, D.M. Sima, S. Van, Huffel Tumor, Segmentation from multimodal MRI using random forest with superpixel and tensor based feature extraction, in: BrainLes 2017: Brainlesion: Glioma, Multiple Sclerosis, Stroke and Traumatic Brain Injuries, 2018, pp. 463–473.
[63] H.N. Bharath, Tensor Based Approaches in Magnetic Resonance Spectroscopic Imaging and Multi-parametric MRI Data Analysis, 2018.
[64] Ö. Çiçek, A. Abdulkadir, S.S. Lienkamp, T. Brox, O. Ronneberger, 3D u-net: learning dense volumetric segmentation from sparse annotation, Medical Image Computing and Computer-Assisted Intervention 9901 (2016) 424–432.
[65] O. Ronneberger, P. Fischer, T. Brox, U-Net: Convolutional networks for biomedical image segmentation, Medical Image Computing and Computer-Assisted Intervention 9351 (2015) 234–241.

[66] L. Sun, W. Ma, X. Ding, Y. Huang, D. Liang, J. Paisley, A 3D spatially weighted network for segmentation of brain tissue from MRI, IEEE Transactions on Medical Imaging 39 (4) (2020) 898–909.
[67] A.M. Mendrik, K.L. Vincken, H.J. Kuijf, M. Breeuwer, W.H. Bouvy, J. de Bresser, A. Alansary, M. de Bruijne, A. Carass, A. El-Baz, A. Jogh, R. Katyal, A.R. Khan, F. van der Lijn, Q. Mahmood, R. Mukherjee, A. van Opbroek, S. Paneri, S. Pereira, M. Persson, M. Rajchl, D. Sarikayan, O. Smedby, C.A. Silva, H.A. Vrooman, S. Vyas, C. Wang, L. Zhaon, G.J. Biessels, M.A. Viergever, MRBrainS challenge: online evaluation framework for brain image segmentation in 3T MRI scans, Computational Intelligence and Neuroscience (2015) 1–16.
[68] A.W. Toga, P.M. Thompson, The role of image registration in brain mapping, Image and Vision Computing 19 (1–2) (2001) 3–24.
[69] K. Mills, C. Tamnes, Methods and considerations for longitudinal structural brain imaging analysis across development, Developmental Cognitive Neuroscience 9 (2014) 172–190.
[70] N. Lepore, C. Brun, Y. Chou, M. Chiang, R.A. Dutton, K.M. Hayashi, E. Luders, O.L. Lupez, H.J. Aizenstein, A.W. Toga, J.T. Becker, P.M. Thompson, Generalized tensor-based morphometry of HIV/AIDS using multivariate statistics on deformation tensors, IEEE Transactions on Medical Imaging 27 (1) (2008) 129–141.
[71] A.D. Leow, I. Yanovsky, M. Chiang, A.D. Lee, A.D. Klunder, A. Lu, J.T. Becker, S.W. Davis, A.W. Toga, P.M. Thompson, Statistical properties of Jacobian maps and the realization of unbiased large-deformation nonlinear image registration, IEEE Transactions on Medical Imaging 26 (6) (2007) 822–832.
[72] A. Leow, I. Yanovsky, N. Parikshak, X. Hua, S. Lee, A. Toga, C. Jack, M. Bernstein, P. Britson, J. Gunter, C. Ward, B. Borowski, L. Shaw, J. Trojanowski, A. Fleisher, D. Harvey, J. Kornak, N. Schuff, G. Alexander, M. Weiner, P.M. Thompson, Alzheimer's disease neuroimaging initiative: a one-year follow up study using tensor-based morphometry correlating degenerative rates, biomarkers and cognition, NeuroImage 45 (3) (2009) 645–655.
[73] M. Chiang, R. Dutton, K.M. Hayashi, O. Lopez, H. Aizenstein, A. Toga, J. Becker, P. Thompson, 3D pattern of brain atrophy in HIV/AIDS visualized using tensor-based morphometry, NeuroImage 34 (1) (2007) 44–60.
[74] E.M. Meintjes, K.L. Narr, A.J.W. Van Der Kouwe, C.D. Molteno, T. Pirnia, B. Gutman, R.P. Woods, P.M. Thompson, J.L. Jacobson, S.W. Jacobson, A tensor-based morphometry analysis of regional differences in brain volume in relation to prenatal alcohol exposure, NeuroImage: Clinical 5 (2014) 152–160.
[75] C. Stamile, F. Cotton, D. Sappey-Marinier, S. Van Huffel, Constrained tensor decomposition for longitudinal analysis of diffusion imaging data, IEEE Journal of Biomedical and Health Informatics 24 (4) (2020) 1137–1148.
[76] M. Boussé, O. Debals, L. De Lathauwer, A tensor-based method for large-scale blind source separation using segmentation, IEEE Transactions on Signal Processing 65 (2) (2017) 346–358.
[77] H. Becker, L. Albera, P. Comon, M. Haardt, G. Birot, F. Wendling, M. Gavaret, C.G. Bénar, I. Merlet, EEG extended source localization: tensor-based vs. conventional methods, NeuroImage 96 (2014) 143–157.
[78] C. Chatzichristos, E. Kofidis, M. Morante, S. Theodoridis, Blind fMRI source unmixing via higher-order tensor decompositions, Journal of Neuroscience Methods 315 (2019) 17–47.

[79] J. Pérez Outeiral, S. Elcoroaristizabal, J.M. Amigo, M. Vidal, Development and validation of a method for the determination of regulated fragrance allergens by high-performance liquid chromatography and parallel factor analysis 2, Journal of Chromatography A 1526 (2017) 82–92.
[80] F. Van Eeghem, L. De Lathauwer, Second-order tensor-based convolutive ICA: deconvolution versus tensorization, in: 2017 IEEE International Conference on Acoustics, Speech and Signal Processing (ICASSP), 2017, pp. 2252–2256.
[81] A. Erol, S. Van Eyndhoven, S. Koekkoek, P. Kruizinga, B. Hunyadi, Joint estimation of hemodynamic response and stimulus function in functional ultrasound using convolutive mixtures, in: 2020 54th Asilomar Conference on Signals, Systems and Computers, 2020, pp. 246–250.
[82] S. Kouchaki, Tensor based source separation for single and multichannel signals, 2015.
[83] A.C.K. Soong, Z.J. Koles, Principal-component localization of the sources of the background EEG, IEEE Transactions on Biomedical Engineering 42 (1) (2001) 59–67.
[84] E. Urrestarazu, J. Iriarte, M. Alegre, M. Valencia, C. Viteri, J. Artieda, Independent component analysis removing artifacts in ictal recordings, Epilepsia 45 (9) (2004) 1071–1078.
[85] B. Hunyadi, P. Dupont, W. Van Paesschen, S. Van Huffel, Tensor decompositions and data fusion in epileptic electroencephalography and functional magnetic resonance imaging data, Wiley Interdisciplinary Reviews: Data Mining and Knowledge Discovery 7 (1) (2017) e1197.
[86] R. Bro, PARAFAC. Tutorial and applications, Chemometrics and Intelligent Laboratory Systems 38 (2) (1997) 149–171.
[87] H. Cole, W. Ray, EEG correlates of emotional tasks related to attentional demands, International Journal of Psychophysiology 3 (1) (1985) 33–41.
[88] J. Möcks, Decomposing event-related potentials: a new topographic components model, Biological Psychology 26 (1–3) (1988) 199–215.
[89] F. Miwakeichi, E. Martínez-Montes, P. Valdés-Sosa, N. Nobuaki, H. Mizuhara, Y. Yamaguchi, Decomposing EEG data into space-time-frequency components using parallel factor analysis, NeuroImage 22 (3) (2004) 1035–1045.
[90] M. De Vos, A. Vergult, L. De Lathauwer, W. De Clercq, S. Van Huffel, P. Dupont, A. Palmini, W. Van Paesschen, Canonical decomposition of ictal scalp EEG reliably detects the seizure onset zone, NeuroImage 37 (3) (2007) 844–854.
[91] M. Mørup, L. Hansen, C. Herrmann, J. Parnas, S.M. Arnfred, Parallel factor analysis as an exploratory tool for wavelet transformed event-related EEG, NeuroImage 29 (3) (2006) 938–947.
[92] C. Tangwiriyasakul, I. Premoli, L. Spyrou, R.F.M. Chin, J. Escudero, M.P. Richardson, Tensor decomposition of TMS-induced EEG oscillations reveals data-driven profiles of antiepileptic drug effects, Scientific Reports 9 (1) (2019) 17057.
[93] W. Juan, X. Li, C. Lu, L. Voss, J. Barnard, J. Sleigh, Characteristics of evoked potential multiple EEG recordings in patients with chronic pain by means of parallel factor analysis, Computational & Mathematical Methods in Medicine (2012) 279560.
[94] M. Hssayeni, T. Wilcox, B. Ghoraani, Tensor decomposition of functional near-infrared spectroscopy (fNIRS) signals for pattern discovery of cognitive response in infants, in: 2020 42nd Annual International Conference of the IEEE Engineering in Medicine and Biology Society (EMBC), 2020, pp. 394–397.
[95] A. Singh, S. Trevick, The epidemiology of global epilepsy, Neurologic Clinics 34 (4) (2016) 837–847.

[96] C. Nagesh, S. Kumar, R. Menon, B. Thomas, A. Radhakrishnan, C. Kesavadas, The imaging of localization related symptomatic epilepsies: the value of arterial spin labelling based magnetic resonance perfusion, Korean Journal of Radiology 19 (5) (2018) 965–977.
[97] B. Litt, R. Esteller, J. Echauz, M. D'Alessandro, R. Shor, T. Henry, P. Pennell, C. Epstein, R. Bakay, M. Dichter, G. Vachtsevanos, Epileptic seizures may begin hours in advance of clinical onset: a report of five patients, Neuron 30 (1) (2001) 51–64.
[98] R. Bro, H. Kiers, A new efficient method for determining the number of components in PARAFAC models, Journal of Chemometrics 17 (5) (2003) 274–286.
[99] E. Acar, C. Bingol, H. Bingol, B. Yener, Computational analysis of epileptic focus localization, in: Proceedings of the Fourth IASTED International Conference on Biomedical Engineering, 2006.
[100] E. Acar, C. Bingol, H. Bingol, R. Bro, B. Yener, Multiway analysis of epilepsy tensors, Bioinformatics 23 (13) (2007), I10–I18.
[101] W. Deburchgraeve, P.J. Cherian, M. De Vos, R.M. Swarte, J.H. Blok, G.H. Visser, P. Govaert, S. Van Huffel, Neonatal seizure localization using PARAFAC decomposition, Clinical Neurophysiology Official Journal of the International Federation of Clinical Neurophysiology 120 (10) (2009) 1787–1796.
[102] W. Deburchgraeve, P.J. Cherian, M. De Vos, R.M. Swarte, J.H. Blok, G.H. Visser, P. Govaert, S. Van Huffel, Automated neonatal seizure detection mimicking a human observer reading EEG, Clinical Neurophysiology 119 (11) (2008) 2447–2454.
[103] B. Hunyadi, D. Camps, L. Sorber, W. Van Paesschen, M. de Vos, S. Van Huffel, L. De Lathauwer, Block term decomposition for modelling epileptic seizures, EURASIP Journal on Advances in Signal Processing (2014) 1–19.
[104] Y.R. Aldana, B. Hunyadi, E.J.M. Reyes, V.R. Rodríguez, S. Van Huffel, Nonconvulsive epileptic seizure detection in scalp EEG using multiway data analysis, IEEE Journal of Biomedical and Health Informatics (2019) 660–671.
[105] E. Acar, C. Bingol, H. Bingol, R. Bro, B. Yener, Seizure recognition on epilepsy feature tensor, in: Annual International Conference of the IEEE Engineering in Medicine and Biology Society, 2007, pp. 4273–4276.
[106] B. Direito, C. Teixeira, B. Ribeiro, M. Castelo-Branco, A. Dourado, Space time frequency (STF) code tensor for the characterization of the epileptic preictal stage, in: 2012 Annual International Conference of the IEEE Engineering in Medicine and Biology Society, 2012, pp. 621–624.
[107] L.Q. Uddin, Complex relationships between structural and functional brain connectivity, Trends in Cognitive Sciences 17 (12) (2013) 600–602.
[108] G. Leismanm, A. Moustafa, T. Shafir, Thinking, walking, talking: The development of integratory brain function, Frontiers in Public Health 4 (2016) 94.
[109] Z. Zhang, G.I. Allen, H. Zhu, D. Dunson, Tensor network factorizations: relationships between brain structural connectomes and traits, NeuroImage 197 (2019) 330–343.
[110] G.I. Allen, Sparse higher-order principal components analysis, in: Proceedings of the Fifteenth International Conference on Artificial Intelligence and Statistics, vol. 22, 2012, pp. 27–36.
[111] R. Prabhakaran, S.E. Blumstein, E.B. Myers, E. Hutchison, B. Britton, An event-related fMRI investigation of phonological-lexical competition, Neuropsychologia 44 (12) (2006) 2209–2221.
[112] K. Glomb, A. Ponce-Alvarez, M. Gilson, P. Ritter, G. Deco, Resting state networks in empirical and simulated dynamic functional connectivity, NeuroImage 159 (2017) 388–402.

[113] A. Kraskov, H. Stögbauer, P. Grassberger, Estimating mutual information, Physical Review E 69 (2004) 066138.
[114] F. Mokhtari, R.E. Mayhugh, C.E. Hugenschmidt, W.J. Rejeski, P.J. Laurienti, Tensor-based vs. matrix-based rank reduction in dynamic brain connectivity, in: Proceedings of the SPIE Medical Imaging Conference, 2018, p. 10574.
[115] N. Leonardi, D. Van de Ville, Identifying network correlates of brain states using tensor decompositions of whole-brain dynamic functional connectivity, 2013 International Workshop on Pattern Recognition in Neuroimaging (2013) 74–77.
[116] F. Mokhtari, P.J. Laurienti, W.J. Rejeski, G. Ballard, Dynamic functional magnetic resonance imaging connectivity tensor decomposition: a new approach to analyze and interpret dynamic brain connectivity, Brain Connectivity 9 (1) (2019) 95–112.
[117] A.G. Mahyari, D.M. Zoltowski, E.M. Bernat, S. Aviyente, A tensor decomposition-based approach for detecting dynamic network states from EEG, IEEE Transactions on Biomedical Engineering 64 (1) (2017) 225–237.
[118] E. Ceulemans, H.A. Kiers, Selecting among three-mode principal component models of different types and complexities: a numerical convex hull based method, British Journal of Mathematical and Statistical Psychology 59 (1) (2006) 133–150.
[119] K. Ye, L. Lim, Schubert varieties and distances between subspaces of different dimensions, SIAM Journal on Matrix Analysis and Applications 37 (3) (2016) 1176–1197.
[120] L. Spyrou, M. Parra, J. Escudero, Complex tensor factorization with PARAFAC2 for the estimation of brain connectivity from the EEG, IEEE Transactions on Neural Systems and Rehabilitation Engineering 27 (1) (2018) 1–12.
[121] K.H. Madsen, N.W. Churchill, M. Mørup, Quantifying functional connectivity in multi-subject fMRI data using component models, Human Brain Mapping 38 (2) (2016) 882–899.
[122] B. Pester, C. Ligges, L. Leistritz, H. Witte, K. Schiecke, Advanced insights into functional brain connectivity by combining tensor decomposition and partial directed coherence, PLoS ONE 10 (6) (2015) e0129293.
[123] M.F. Pagnotta, G. Plomp, Time-varying MVAR algorithms for directed connectivity analysis: critical comparison in simulations and benchmark EEG data, PLoS ONE 13 (6) (2018) e0198846.
[124] E. Karahan, P.A. Rojas-López, M.L. Bringas-Vega, P.A. Valdés-Hernández, P.A. Valdes-Sosa, Tensor analysis and fusion of multimodal brain images, Proceedings of the IEEE 103 (9) (2015) 1531–1559.
[125] S. Bressler, A. Seth, Wiener–granger causality: a well established methodology, NeuroImage 58 (2) (2010) 323–329.
[126] P. McCullagh, J.A. Nelder, Generalized Linear Models (Mono-Graphs on Statistics and Applied Probability), Chapman & Hall, London, 1983.
[127] H. Zhou, L. Li, H. Zhu, Tensor regression with applications in neuroimaging data analysis, Journal of the American Statistical Association 108 (502) (2013) 540–552.
[128] X. Li, D. Xu, H. Zhou, L. Li. Tucker, Tensor regression and neuroimaging analysis, Statistics in Biosciences 10 (2018) 520–545.
[129] W.W. Sun, L. Li, STORE: sparse tensor response regression and neuroimaging analysis, Journal of Machine Learning Research 18 (2017) 1–37.
[130] Q. Zhao, C.F. Caiafa, D. Mandic, L. Zhang, T. Ball, A. Schulze-Bonhage, A. Cichocki, Multilinear subspace regression: an orthogonal tensor decomposition approach, in: Advances in Neural Information Processing Systems (NIPS), 2011, pp. 1269–1277.

[131] C.F.V. Latchoumane, F. Vialatte, J. Solé-Casals, M. Maurice, S. Wimalaratna, N. Hudson, J. Jeong, A. Cichocki, Multiway array decomposition analysis of EEGs in Alzheimer's disease, Journal of Neuroscience Methods 207 (1) (2012) 41–50.
[132] D. Qian, B. Wang, X. Qing, T. Zhang, Y. Zhang, X. Wang, M. Nakamura, Bayesian nonnegative CP decomposition-based feature extraction algorithm for drowsiness detection, IEEE Transactions on Neural Systems and Rehabilitation Engineering 25 (8) (2017) 1297–1308.
[133] J. Escudero, E. Acar, A. Fernández, R. Bro, Multiscale entropy analysis of resting-state magnetoencephalogram with tensor factorisations in Alzheimer's disease, Brain Research Bulletin 119 (2015) 136–144.
[134] F. Song, A.H. Phan, Q. Zhao, T. Huttunen-Scott, J. Kaartinen, T. Ristaniemi, H. Lyytinen, A. Cichocki, Benefits of multi-domain feature of mismatch negativity extracted by non-negative tensor factorization from EEG collected by low-density array, International Journal of Neural Systems 22 (6) (2012) 1250025.
[135] Y. Wang, L. Yuan, J. Shi, A. Greve, J. Ye, A. Toga, P. Thompson, Applying tensor-based morphometry to parametric surfaces can improve MRI-based disease diagnosis, NeuroImage 74 (2013) 209–230.
[136] A. Rezeika, M. Benda, P. Stawicki, F. Gembler, A. Saboor, I. Volosyak, Brain-computer interface spellers: a review, Brain Sciences 8 (4) (2018) 57.
[137] A.H. Phan, A. Cichocki, Tensor decompositions for feature extraction and classification of high dimensional datasets, Nonlinear Theory and Its Applications, IEICE 1 (1) (2010) 37–68.
[138] H. Ramoser, J. Muller-Gerking, G. Pfurtscheller, Optimal spatial filtering of single trial EEG during imagined hand movement, IEEE Transactions on Rehabilitation Engineering 8 (4) (2000) 441–446.
[139] A. Cichocki, Y. Washizawa, T. Rutkowski, H. Bakardjian, A.H. Phan, S. Choi, H. Lee, Q. Zhao, L. Zhang, Y. Li, Noninvasive BCIs: multiway signal-processing array decompositions, Computer 41 (10) (2008) 34–42.
[140] B. Hunyadi, M. Signoretto, S. Debener, S. Van Huffel, M. de Vos, Classification of structured EEG tensors using nuclear norm regularization: improving P300 classification, in: 2013 International Workshop on Pattern Recognition in Neuroimaging, Philadelphia, 2013, pp. 98–101.
[141] A. Onishi, A.H. Phan, K. Matsuoka, A. Cichocki, Tensor classification for P300-based brain computer interface, in: 2012 IEEE International Conference on Acoustics, Speech and Signal Processing (ICASSP), 2012, pp. 581–584.
[142] R. Zink, B. Hunyadi, S. Van Huffel, M. de Vos, Tensor-based classification of an auditory mobile BCI without a subject-specific calibration phase, Journal of Neural Engineering 13 (2) (2016) 026005.
[143] E. Kinney-Lang, A. Ebied, J. Escudero, Building a tensor framework for the analysis and classification of steady-state visual evoked potentials in children, in: 2018 26th European Signal Processing Conference (EUSIPCO), vol. 21(6), 2018, pp. 296–300.
[144] Y. Zhang, G. Zhou, J. Jin, M. Wang, X. Wang, A. Cichocki, L1-regularized multiway canonical correlation analysis for SSVEP-based BCI, IEEE Transactions on Neural Systems and Rehabilitation Engineering 21 (6) (2013) 887–896.
[145] N. Vervliet, O. Debals, L. Sorber, M. Van Barel, L. De Lathauwer, Tensorlab 3.0, Available online https://www.tensorlab.net, Mar. 2016.
[146] C. Orphanidou, A review of big data applications of physiological signal data, Biophysical Reviews 11 (1) (2019) 83–87.

[147] J. Schmidhuber, Deep learning in neural networks: an overview, Neural Networks 61 (2015) 85–117.
[148] W. Samek, G. Montavon, A. Vedaldi, L.K. Hansen, K.-R. Müller, Explainable AI: Interpreting, Explaining and Visualizing Deep Learning, Springer, 2019, p. 11700.
[149] A. Cichocki, A.H. Phan, Q. Zhao, N. Lee, I.V. Oseledets, M. Sugiyama, D. Mandic, Tensor networks for dimensionality reduction and large-scale optimizations: part 2 applications and future perspectives, arXiv preprint, arXiv:1708.09165, 2017.
[150] N.D. Sidiropoulos, L. De Lathauwer, X. Fu, K. Huang, E.E. Papalexakis, C. Faloutsos, Tensor decomposition for signal processing and machine learning, IEEE Transactions on Signal Processing 65 (13) (2017) 3551–3582.
[151] I. Oseledets, Tensor-train decomposition, SIAM Journal on Scientific and Statistical Computing 33 (5) (2011) 2295–2317.
[152] X. Xu, Q. Wu, S. Wang, J. Liu, J. Sun, A. Cichocki, Whole brain fMRI pattern analysis based on tensor neural network, IEEE Access 6 (2018) 29297–29305.
[153] B. Hunyadi, M. Signoretto, W. Van Paesschen, J.A.K. Suykens, S. Van Huffel, M. De Vos, Incorporating structural information from the multichannel EEG improves patient-specific seizure detection, Clinical Neurophysiology 123 (12) (2012) 2352–2361.
[154] M. Signoretto, Q.T. Dinh, L. De Lathauwer, J.A.K. Suykens, Learning with tensors: a framework based on convex optimization and spectral regularization, Machine Learning 94 (3) (2014) 303–351.
[155] S. Van Eyndhoven, P. Dupont, S. Tousseyn, N. Vervliet, W. Van Paesschen, S. Van Huffel, B. Hunyadi, Augmenting interictal mapping with neurovascular coupling biomarkers by structured factorization of epileptic EEG and fMRI data, arXiv preprint, arXiv: 2004.14185, 2020.
[156] E.A. Ashley, Towards precision medicine, Nature Reviews. Genetics 17 (9) (2016) 507–522.
[157] N. Dron, R.F.M. Chin, J. Escudero, Canonical polyadic and block term decompositions to fuse EEG, phenotypic scores, and structural MRI of children with early-onset epilepsy, in: 2020 28th European Signal Processing Conference (EUSIPCO), 2020, pp. 1145–1149.
[158] M.M.G. Ricci, T. Levi-Civita, Méthodes de calcul différentiel absolu et leurs applications, Mathematische Annalen 54 (1900) 125–201.
[159] A. Cichocki, D. Mandic, L. De Lathauwer, G. Zhou, Q. Zhao, C.F. Caiafa, A. Phan, Tensor decompositions for signal processing applications: from two-way to multiway component analysis, IEEE Signal Processing Magazine 32 (2) (2015) 145–163.

Tensors for Data Processing

Theory, Methods, and Applications

Edited by Yipeng Liu

As a higher-order generalization of a matrix, a tensor is a natural representation for multidimensional data; tensor-based processing can avoid multilinear data structure loss that occurs in classical matrix-based data processing methods. The move from matrix to tensor is beneficial for many diverse application areas, including signal processing, machine learning, computer vision, acoustics, neuroscience, communication, medical engineering, seismology, psychometrics, chemometrics, biometrics, quantum physics, and quantum chemistry.

Tensors for Data Processing: Theory, Methods, and Applications covers both classical and state-of-the-art parts of computation theories, processing methods, performance analysis, and engineering applications, with an emphasis on techniques for data processing.

This reference is ideal for students, researchers, and industry developers who want to understand and use tensor-based data processing theories and methods.

Key Features

- A friendly tutorial of tensor representations, computations, and decompositions
- A series of detailed tensor-based data processing methods
- A wide range of applications from different disciplines

About the Editor

Yipeng Liu is an associate professor with the School of Information and Communication Engineering, University of Electronic Science and Technology of China (UESTC), Chengdu, China.

ELSEVIER

ACADEMIC PRESS
An imprint of Elsevier
elsevier.com/books-and-journals

ISBN 978-0-12-824447-0